140 (2022) 213043

Contents lists available at ScienceDirect

Biomaterials Advances

journal homepage: www.journals.elsevier.com/materials-science-and-engineering-c

Three-armed RGD-decorated *star*PLA-PEG nanoshuttle for docetaxel delivery

Serena Maria Torcasio [a,b], Roberto Oliva [a], Monica Montesi [c,*], Silvia Panseri [c], Giada Bassi [c], Antonino Mazzaglia [d], Anna Piperno [a], Olivier Coulembier [b], Angela Scala [a,*]

[a] *Department of Chemical, Biological, Pharmaceutical and Environmental Sciences, University of Messina, V.le F. Stagno d'Alcontres 31, 98166 Messina, Italy*
[b] *Center of Innovation and Research in Materials and Polymers (CIRMAP), Laboratory of Polymeric and Composite Materials, University of Mons, Place du Parc 23, 7000 Mons, Belgium*
[c] *CNR-ISTEC, Institute of Science and Technology for Ceramics, National Research Council of Italy, Via Granarolo 64, 48018 Faenza, RA, Italy*
[d] *CNR-ISMN, Istituto per lo Studio dei Materiali Nanostrutturati, URT of Messina c/o Department of Chemical, Biological, Pharmaceutical and Environmental Sciences of the University of Messina, V.le F. Stagno d'Alcontres 31, 98166, Messina, Italy*

ARTICLE INFO

Keywords:
Star polymer
Polylactide
Scratch test
Docetaxel
CuAAC

ABSTRACT

A novel *star*-shaped amphiphilic copolymer based on three poly(lactide)-*block*-poly(ethylene glycol) (PLA-PEG) terminal arms extending from a glycerol multifunctional *core* was newly synthesized and decorated with the tumor-targeting ligand cyclic-RGDyK peptide (Arg-Gly-Asp-D-Tyr-Lys) to be eventually formulated in polymeric micelles incorporating a suitable anticancer drug (*i.e.,* Docetaxel, DTX; drug loading 16 %, encapsulation efficiency 69 %). The biological profile of unloaded micelles (**RGD-NanoStar**) was studied on Human Adipose-derived Mesenchymal Stem Cells (Ad-MSCs) as health control, pointing out the absence of toxicity. Surprisingly, an unprecedented effect on cell viability was exerted by **RGD-NanoStar**, comparable to that of the free DTX, on tumoral MDA-MB 468 Human Breast Adenocarcinoma cells, specifically starting from 48 h of culture (about 40 % and 60 % of dead cells at 48 and 72 h, respectively, at all tested concentrations). **RGD-NanoStar** reduced the cell viability also of tumoral U87 Human Glioblastoma cells, compared to cells only, at 72 h (about 25 % of dead cells) demonstrating a time-dependent effect exerted by the highest concentrations. The effects of DTX-loaded micelles (**RGD-NanoStar/DTX**) on U87 and MDA-MB 468 cell lines were evaluated by MTT, cell morphology analysis, and scratch test. A compromised cell morphology was observed without significant difference between DTX-treated and **RGD-NanoStar/DTX** – treated cells, especially in U87 cell line. Although no apparent benefit emerged from the drug incorporation into the nanosystem by MTT assay, the scratch test revealed a statistically significant inhibition of tumoral cell migration on both cell lines, confirming the well-known role of DTX in inhibiting cell movements even when loaded on polymeric micelles. Specifically, only 43 μm distance was covered by U87 cells after 30 h culture with **RGD-NanoStar/DTX** (30 μg/mL) compared to 73 μm in the presence of free DTX at the same concentration; more interestingly, a total absence of MDA-MB 468 cell movements was detected at 30 h compared to about 50 μm distance covered by cells in the presence of free DTX (10 μg/mL). The stronger inhibitory activity on cell migration of **RGD-NanoStar/DTX** compared to the free drug in both cell lines at 30 h attested for a good ability of the drug-loaded nanocarrier to reduce tumor propagation and invasiveness, enhancing the typical effect of DTX on metastatization.

1. Introduction

Star polymers based on amphiphilic polylactide-poly(ethylene glycol) (PLA-PEG) are biomaterials of growing interest in nanomedicine [1]. Their exclusive structure, consisting of multiple variable-length linear chains (*arms*) radiating from a central *core*, is responsible for remarkable properties unattainable by their linear equivalents. Owing to their typical architecture, *star*-shaped polymers exhibit smaller hydrodynamic radius and lower viscosity compared with conventional linear analogs of the same molecular weight and composition, and display peculiar morphologies, thermal and rheological properties, and degradation profiles [2,3]. Furthermore, *star* polymers combine a three-

* Corresponding authors.
E-mail addresses: monica.montesi@istec.cnr.it (M. Montesi), ascala@unime.it (A. Scala).

https://doi.org/10.1016/j.bioadv.2022.213043
Received 21 April 2022; Received in revised form 17 July 2022; Accepted 19 July 2022
Available online 25 July 2022

dimensional spherical and compact shape with a high density of functionalizable end-groups and a covalently reinforced *core-shell* structure similar to that of micelles that avoids disassembly when diluted. Their unique shape and attractive properties, such as encapsulation capability, internal and peripheral functionality, high arm density, efficient synthesis and enhanced stimuli-responsiveness make them promising tools in various field, including drug and gene delivery [4–7] and tissue engineering [8,9]. Specifically, micelles self-assembled from biodegradable *star*-shaped PLA-PEG copolymers, with a unique three-dimensional shape and a highly branched structure, can provide spacious harbor for encapsulating therapeutic agents, owning a low critical micelle concentration (CMC) which results in longer blood circulation time after intravenous injection. Due to these powerful properties, several *star*-shaped architectures have been achieved with highly controlled structures through the advancements in living polymerization techniques combined with the well-known advantages of *click* chemistry reactions [10–12], leading the field of *star* polymers to quickly expand in terms of advanced and smart functional materials [1–3].

In the framework of our studies dealing with the development of polymeric nanomaterials for drug delivery purposes [13–16], we have designed and synthesized a novel three arms amphiphilic *star*PLA-PEG copolymer decorated with cyclic-RGDyK peptide (RGD) and nanoformulated in micelles incorporating the anticancer drug Docetaxel (DTX) (Fig. 1).

The *star*PLA-PEG was obtained in a multi-step synthesis by sequentially combining a typical ring-opening polymerization (ROP) of lactide, using glycerol as the *core*, with proper copper-catalyzed azide-alkyne cycloaddition (CuAAC) reactions to functionalize the three arms of PLA with suitable components (*i.e.,* PEG and RGD) for drug delivery purposes. RGD peptide was selected as a tumor targeting ligand able to selectively recognize and bind with high affinity $\alpha_v\beta_3$ integrins, which are overexpressed on invasive tumors, such as melanomas and glioblastomas, but also on breast, ovarian, prostate cancers [17–18]. Moreover, it plays a regulator role in tumor-induced angiogenesis, ensuring endothelial cell survival, and in tumor metastasis. The use of RGD as integrin ligand represents an appealing strategy to design selective drug nanocarriers, since integrins are surface receptors exhibiting extracellular binding domains; thus, they have a favorable location to be readily accessible by the targeted drug delivery system (DDS) in the extracellular compartment. Moreover, they promote internalization upon ligand binding, so that the DDS can enter its targeted cell by receptor-mediated endocytosis and then traffic to intracellular endosomes and/or lysosomes, allowing the drug to be released into the cytoplasm [18].

DTX is a lipophilic semi-synthetic taxane approved by the Food and Drug Administration (FDA) for the treatment of different types of cancer, such as breast, ovarian, prostate, non-small-cell lung cancer, and gastric adenocarcinoma. DTX is a cytostatic drug acting by reversibly binding to microtubules, promoting transitory structure stabilization, leading to cell cycle arrest [19]. DTX is also considered as one of the most effective chemotherapeutic agents for the treatment of metastatic tumors, owning promising results in metastatic glioblastoma treatment, and it is 1.2–1.3-fold more potent in metastasized breast cancer than common agents like paclitaxel [20–23]. Cells of metastatic tumors, such as glioblastoma and adenocarcinoma, have a highly marked migration ability which allows them to disseminate from the primary tumor mass and to colonize distant organs reaching the metastatic state, which accounts for >90 % of all cancer related deaths. The migrative process involves precise coordination of cell movements by the formation of invasive protrusions (*i.e.,* filopodia, pseudopodia, lobopodian and lamellipodia based on the shape) [24]. DTX was suggested to be involved in suppressing filopodia formation of tumor cells with subsequent migration and invasion reduction [25–26]. However, the clinical use of intravenous DTX (Taxotere® Sanofi Aventis) is limited by its high lipophilicity, poor aqueous solubility (4.93 μg/mL) and low bioavailability. Therefore, different types of DDS and nanoformulations have been developed to overcome these drawbacks [26–34]. In the present study, DTX was efficiently encapsulated into the *star*PLA-PEG-RGD micelles by nanoprecipitation and the physicochemical properties of both "empty" (**RGD-NanoStar**) and drug-loaded (**RGD-NanoStar/DTX**) micelles were evaluated in terms of CMC, size and zeta potential. The cytotoxicity, the antitumoral efficiency and the inhibition of tumoral cell migration were studied *in vitro* on Human Adipose-derived Mesenchymal Stem Cells (Ad-MSCs) as health control and on two different tumoral cell lines (*i.e.,* U87 Human Glioblastoma and MDA-MB 468 Human Breast Adenocarcinoma) as models of two most common primary and metastatic tumors affecting people worldwide.

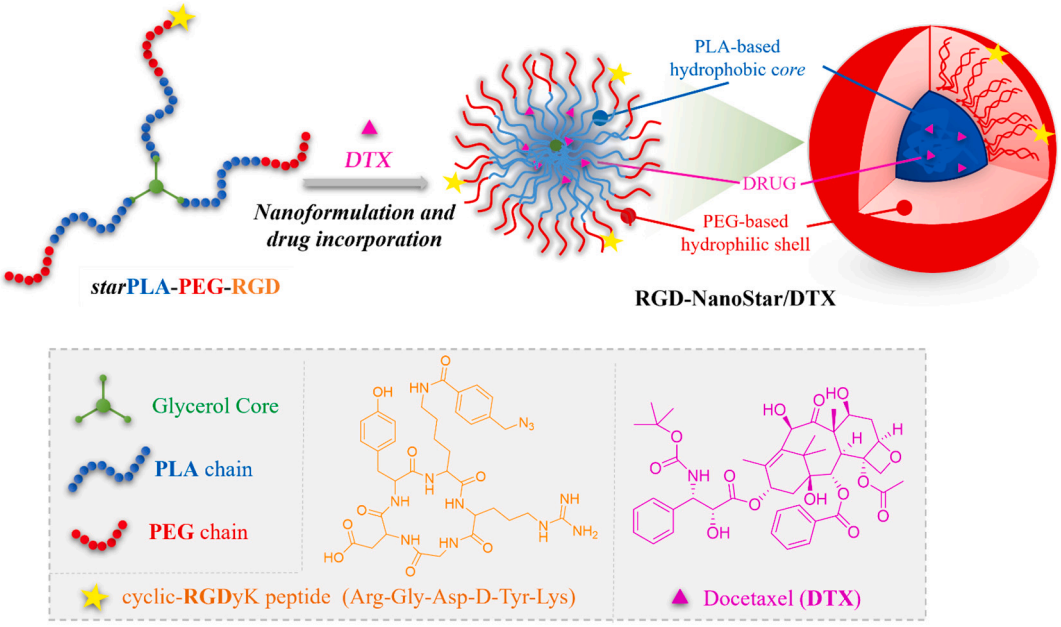

Fig. 1. Sketched view of the self-assembly in aqueous solution of *star*PLA-PEG-RGD and DTX incorporation, leading to **RGD-NanoStar/DTX**. In the inset all the components of the polymeric micelles are depicted.

2. Experimental

2.1. Synthesis of starPLA-PEG-RGD

The target compound was synthesized by a multi-step procedure consisting of: ROP of lactide monomer initiated by glycerol; alkynylation of *star*PLA; CuAAC reaction with mono-azide PEG; alkynylation of *star*PLA-PEG; final CuAAC reaction with azide-RGD peptide.

2.1.1. Synthesis of starPLA (3)

An initial [lactide (L-LA)]$_0$/[initiator]$_0$/[DBU]$_0$ ratio of 97/1/2 ([L-LA]$_0$ = 1 M) has been selected to obtain a *star*PLA (**3**) with a molecular weight of 14.000 g/mol. In a glove box under nitrogen pressure, glycerol (**1**) (6.6 mg, 7•10^{-5} mol, 1 equiv) and DBU (21.8 mg, 1.4•10^{-4} mol, 2 equiv) were solubilized in 2 mL of anhydrous DCM into a glass vial. L-Lactide (**2**) (1 g, 6.9•10^{-3} mol, 97 polymerization degree) was solubilized in 5 mL of anhydrous DCM into another glass vial and then added to the first solution. The reaction was left to stir 12 min, and then benzoic acid (21 mg, 1.7•10^{-4} mol, 2.4 equiv) dissolved in 0.2 mL of anhydrous DCM was added to stop the polymerization. The vial was taken out of glove box, the solution was transferred into a round bottom flask to reduce the volume under vacuum. The solution was precipitated into cold technical methanol, centrifuged and dried for 5 h into a vacuum oven at 60 °C to give 980 mg (98 % yield) of starPLA (**3**) as a white powder. ^{1}H NMR (500 MHz, $CDCl_3$, δ): 1.57 (m, 3H, $[CH_3]_n$), 4.22 (m, 5H, -CH_2CHCH_2), 4.36 (m, 1H, CHOH), 5.15 (m, 1H, $[CH]_n$). Polymerization Degree$^{1H\ NMR}$ = 97, $\bar{M}n^{1H\ NMR}$ = 14.000 g/mol, SEC: $\bar{M}n^{SEC,app}$ = 21.019 g/mol, $Đ_M$ = 1.12.

2.1.2. Synthesis of pentynoic anhydride (5)

Pentynoic acid (**4**) (2 g, 20.4•10^{-3} mol, 2 equiv) and DCC (2.1 g, 10.2•10^{-3} mol, 1 equiv) were solubilized in 20 mL of DCM into a round bottom flask. The solution was left to stir for 12 h, then was filtered on filter paper and the solid was washed two times with 20 mL of DCM. The organic phase was evaporated under vacuum to obtain an oil, that was precipitated into 10 mL of n-hexane to form two liquid phases; the bottom part was recovered with a syringe and then dried under vacuum to obtain 940 mg (26 % yield) of pentynoic anhydride (**5**) as a brown oil. ^{1}H NMR (500 MHz, $CDCl_3$, δ): 2.67 (t, J = 7.2 Hz, 2H, $CH_2CH_2C{\equiv}CH$), 2.47 (dt, J = 7.2 Hz, J = 2.6 Hz, 2H, $CH_2CH_2C{\equiv}CH$), 1.97 (t, 1H, J = 2.6 Hz, C≡CH); ^{13}C NMR (500 MHz, $CDCl_3$, δ): 167.2 (C=O), 81.5 (C≡), 69.7 (≡CH), 34.2 (CH_2), 13.7 (CH_2).

2.1.3. Synthesis of alkynyl-terminated starPLA (6)

StarPLA (**3**) (980 mg, 7•10^{-5} mol, 1 equiv), DMAP (34 mg, 2.77•10^{-4} mol, 4 equiv) and pentynoic anhydride (**5**) (50 mg, 2.77•10^{-4} mol, 4 equiv) were solubilized in 30 mL of DCM into a round bottom flask and left stirring for 12 h at room temperature. The solution was washed three times with a saturated solution of $NaHCO_3$ and three times with a saturated solution of $NaHSO_4$. Organic phases were collected, dried over Na_2SO_4, filtered and concentrated under vacuum. The solution was precipitated into cold technical methanol, centrifuged and dried for 5 h into a vacuum oven at 60 °C to obtain 900 mg (90 % yield) of alkynyl-terminated starPLA (**6**) as a white powder. ^{1}H NMR (500 MHz, $CDCl_3$, δ): 1.57 (m, 3H, $-[CH_3]_n$-), 2.65 (m, 2H, $CH_2CH_2C{\equiv}CH$), 2.52 (m, 2H, $CH_2CH_2C{\equiv}CH$), 1.98 (t, 1H, J = 2.5 Hz, C≡CH), 4.22 (m, 5H, -CH_2CHCH_2-), 5.15 (m, 1H, $-[CH]_n$-). Polymerization Degree$^{1H\ NMR}$ = 97, $\bar{M}n^{1H\ NMR}$ = 14.294 g/mol, SEC: $\bar{M}n^{SEC,app}$ = 21.207 g/mol, $Đ_M$ = 1.13.

2.1.4. Synthesis of mono-tosyl PEG (8)

In a glove box, under nitrogen pressure, PEG diol (**7**) (500 mg, 2.5•10^{-4} mol, 1 equiv) was dissolved in 6.75 mL of dry toluene in a glass vial and vigorously stirred till complete dissolution. Then Ag_2O (87 mg, 3.75•10^{-4} mol, 1.5 equiv) and KI (8.3 mg, 5•10^{-5} mol, 0.2 equiv) were added, and after 15 min of vigorous stirring TsCl (50 mg, 2.63•10^{-4} mol, 1.05 equiv) was added. The reaction was stirred for 16 h in the glove box. The solution was taken out of the glove box, filtered on paper filter and dried under vacuum to obtain 287 mg of a colorless oil. ^{1}H NMR and MALDI-ToF analyses demonstrated that it is a mixture of mono-tosyl PEG (**8**) and unreacted PEG diol (**7**) (ratio 1:1), that was directly used in the next synthetic step, without further purification. ^{1}H NMR (500 MHz, $CDCl_3$, δ): 2.44 (s, 3H, CH_3), 3.64 (m, 4H, $-[CH_2CH_2O]_n$-), 4.15 (t, 2H, J = 5 Hz, CH_2OTs), 7.33 (d, 2H, J = 8.5 Hz, Ar H), 7.79 (d, 2H, J = 8.5 Hz, Ar H).

2.1.5. Synthesis of mono-azide PEG (9)

In a glove box, under nitrogen pressure, the mixture obtained in the previous step (574 mg, containing 6.65•10^{-5} mol of mono-tosyl PEG (**8**), 1 equiv) and NaN_3 (22 mg, 3.33•10^{-4} mol, 5 equiv) were dissolved into 5 mL of anhydrous DMF into a round bottom flask. Then the flask was taken from the glove box and stirred for 12 h into an oil bath at 90 °C. Afterwards, DMF was evaporated under vacuum and the crude product was dissolved in DCM and washed two times with brine and two times with deionized water. Organic phases were collected, dried over Na_2SO_4 and evaporated under vacuum to obtain 120 mg of a white solid. ^{1}H NMR and MALDI-ToF analyses demonstrated that it is a mixture of mono-azide PEG (**9**) and unreacted PEG diol (**7**) (ratio 1:1). ^{1}H NMR (500 MHz, $CDCl_3$, δ): 3.39 (t, 2H, J = 5 Hz, -CH_2N_3), 3.64 (m, 4H, $-[CH_2CH_2O]_n$).

2.1.6. Synthesis of starPLA-PEG (10)

Alkynyl-terminated starPLA (**6**) (650 mg, 4.56•10^{-5} mol, 1 equiv) and the mixture obtained in the previous step (555 mg, containing 1.37•10^{-4} mol of mono-azide PEG (**9**), 3 equiv.) were dissolved in 2 mL of anhydrous THF into a glass vial. Then CuBr (0.65 mg, 4.56•10^{-6} mol, 0.1 equiv) and PMDETA (0.79 mg, 4.56•10^{-6} mol, 0.1 equiv) were added to the reaction mixture. The solution was stirred at room temperature for 16 h. The vial was taken out of glove box and the solvent was evaporated under vacuum. The residue was washed three times with 5 mL of deionized water to remove the unreacted PEG-diol and centrifuged at 2800 rpm for 50 min at 10 °C. The solid was dried at 40 °C in a vacuum oven for 4 h leading to 891 mg (yield 96 %) of starPLA-PEG (**10**). ^{1}H NMR (500 MHz, $CDCl_3$, δ): 1.57 (d, 3H, $-[CH_3]$n-), 2.82 (t, 2H, J = 5 Hz, $CH_2CH_2C_{triazole}$), 3.06 (t, 2H, J = 7.5 Hz, $CH_2N_{triazole}$), 3.64 (m, 4H, $-[CH_2CH_2O]$n-), 4.22 (m, 5H, -CH_2CHCH_2-), 4.49 (t, 2H, J = 5 Hz, $CH_2CH_2C_{triazole}$), 5.15 (m, 1H, $-[CH]_n$-), 7.53 (s, 1H, $CH_{triazole}$). $\bar{M}n^{SEC,app}$ = 32.212 g/mol, $Đ_M$ = 1.14.

2.1.7. Synthesis of alkynyl-terminated starPLA-PEG (11)

StarPLA-PEG (**10**) (891 mg, 4.38•10^{-5} mol, 1 equiv), DMAP (21 mg, 1.73•10^{-4} mol, 4 equiv) and pentynoic anhydride (**5**) (31 mg, 1.73•10^{-4} mol, 4 equiv) were solubilized in 30 mL of DCM into a round bottom flask and the mixture was stirred for 12 h at room temperature. The solution was washed three times with deionized water. Organic phases were collected, dried over Na_2SO_4, filtered and dried under vacuum to obtain 788 mg (88 % yield) of alkynyl-terminated starPLA-PEG (**11**) as a white powder. ^{1}H NMR (500 MHz, $CDCl_3$, δ): 1.57 (d, 3H, $-[CH_3]_n$-), 1.98 (t, 1H, J = 2.7 Hz, C≡CH), 2.52 (dt, 2H, J = 2.7, J = 6.5 Hz, $CH_2CH_2C{\equiv}CH$), 2.67 (t, 2H, J = 6.5 Hz, $CH_2CH_2C{\equiv}CH$), 2.82 (t, 2H, J = 5 Hz, $CH_2CH_2C_{triazole}$), 3.06 (t, 2H, J = 7.5 Hz, $CH_2N_{triazole}$), 3.64 (m, 4H, $-[CH_2CH_2O]_n$-), 4.22 (m, 5H, -CH_2CHCH_2-), 4.27 (t, 2H, J = 5 Hz, OCH_2CH_2OCO), 4.49 (t, 2H, J = 5 Hz, $CH_2CH_2C_{triazole}$), 5.15 (m, 1H, $-[CH]_n$), 7.53 (s, 1H, $CH_{triazole}$). $\bar{M}n^{SEC,app}$ = 34.203 g/mol, $Đ_M$ = 1.16.

2.1.8. Synthesis of starPLA-PEG-RGD (13)

In a glove box, under nitrogen pressure, alkynyl-terminated starPLA-PEG (**11**) (137 mg, 6.18•10^{-6} mol, 1 equiv) and azide-RGD peptide (**12**) (10 mg, 1.23•10^{-5} mol, 2 equiv) were dissolved into 2 mL of anhydrous DMF into a glass vial. Then CuBr (0.1 mg, 6.18•10^{-7} mol, 0.1 equiv) and PMDETA (0.1 mg, 6.18•10^{-7} mol, 0.1 equiv) were added to the reaction mixture. The solution was left under stirring at room temperature for 16

h. The solvent was evaporated under vacuum and then the solid residue was washed two times with deionized water and centrifuged at 2800 rpm for 50 min at 10 °C. Water residues were removed in a vacuum oven at 40 °C for 2 h to obtain 80 mg (54 % yield) of starPLA-PEG-RGD (**13**), as a brown solid. ^{1}H NMR (500 MHz, d_7-DMF, δ): selected peaks 1.53 (d, 3H, $-[CH_3]_n$-), 1.98 (t, 1H, J = 2.7 Hz C≡CH), 2.52 (m, 2H, $CH_2CH_2C{\equiv}CH$), 2.65 (m, 2H, $CH_2CH_2C{\equiv}CH$), 2.82 (t, 2H, J = 5 Hz, $CH_2CH_2C_{triazole}$), 2.99 (m, 2H, $CH_2N_{triazole}$), 3.58 (m, 4H, $-[CH_2CH_2O]_n$-), 4.19 (m, 2H, CH_2), 4.22 (t, 2H, J = 5 Hz, OCH_2CH_2OCO), 4.38 (m, 5H, -CH_2CHCH_2-), 4.56 (t, 2H, J = 5 Hz, $CH_2CH_2C_{triazole}$), 5.28 (m, 1H, $-[CH]_n$), 6.65 (br s, 1H, NH), 6.72 (d, 2H, Ar H, J = 8 Hz), 7.02 (d, 2H, Ar H, J = 8 Hz), 7.39 (s, 1H, $CH_{triazole}$), 7.43 (d, 2H, Ar H, J = 8 Hz), 7.60 (br s, 1H, NH), 7.78 (br s, 1H, NH), 7.97 (d, 2H, ArH, J = 8 Hz), 8.39 (br s, 1H, NH), 8.55 (br s, 1H, NH), 8.74 (br s, 1H, NH).

2.2. Preparation of RGD-NanoStar/DTX and RGD-NanoStar

RGD-NanoStar/DTX micelles were prepared at two different polymer:drug ratios (10:1 and 10:3). To that end, *star*PLA-PEG-RGD (3 mg) blended with *star*PLA-PEG (27 mg) and DTX (3 mg for the 10:1 nanoformulation; 9 mg for the 10:3 nanoformulation) were dissolved in 3 mL of THF. The organic solution was added dropwise to 30 mL of water under stirring. The mixture was then stirred at room temperature for 4 h followed by THF evaporation under vacuum. The solution was gently centrifuged (1500 rpm) and the supernatant was freeze-dried to obtain **RGD-NanoStar/DTX** micelles. Similarly, empty **RGD-NanoStar** micelles were prepared with the same method, without adding the drug, and used as control.

2.3. Drug loading

The drug content in the micelles and the loading efficiency were determined by UV–Vis spectroscopy by an the indirect method measuring the amount of unencapsulated drug recovered in the pellet obtained by the gentle centrifugation. Briefly, the weighed pellet was dissolved in 1 mL of DMSO and the UV–Vis spectrum was recorded. The amount of unencapsulated DTX was calculated at the wavelength of 274 nm. A calibration curve for DTX in DMSO was previously constructed in the concentration range 1237–154 μM. On the basis of optical absorbance data and molar extinction coefficient ($\varepsilon_{274} \cong 1021\ M^{-1}\ cm^{-1}$), drug loading (DL) and encapsulation efficiency (EE) were calculated, for difference, using the following equations:

- DL (%) = (Drug weight in the NPs / weight of the drug-loaded NPs) × 100.
- EE (%) = (Drug weight in the NPs / weight of drug used in the formulation) × 100.

2.4. Evaluation of CMC

The self-assembly of *star*PLA-PEG and *star*PLA-PEG-RGD copolymers was investigated in aqueous solution using pyrene as a probe. The CMC of the two copolymers was determined by fluorescence spectra. To obtain sample solutions, a pyrene solution in acetone (6×10^{-6} M) was prepared and added to a series of vials, followed by acetone evaporation. Then, a polymer solution of an adapted concentration (range 1×10^{-3} - 0.1 mg/mL) was added to the vials. The solutions were equilibrated at room temperature overnight. The fluorescence emission wavelength was fixed at 390 nm, and the emission fluorescence intensities at 338 and 333 nm were monitored. The intensity ratios of I_{338}/I_{333} were plotted as a function of logarithm of two copolymer concentrations. The excitation spectrum red-shift from 333 to 338 nm indicated the transfer of pyrene molecules from an aqueous environment to the hydrophobic micelle core.

2.5. Stability studies

Stability studies were carried out by dispersing **RGD-NanoStar/DTX** (0.3 mg/mL) in ultrapure water and in PBS (0.01 M, pH 7.4). The dispersions were kept under stirring (T = 37 °C) along 7 days and analyzed by DLS. Zeta potential was measured along 1 week on the dispersion prepared in ultrapure water and stored at 37 °C. Data were acquired at t = 0, 3, and 7 days.

2.6. In vitro biological studies on RGD-NanoStar and RGD-NanoStar/DTX

The cytotoxicity of **RGD-NanoStar** was tested on Ad-MSCs as model of healthy cells. **RGD-NanoStar** and **RGD-NanoStar/DTX** were tested on U87 and MDA-MB 468 tumoral cell lines using DTX as positive control and cells only as negative control. Briefly, **RGD-NanoStar/DTX** (1 mg contains 160 μg of DTX and 840 μg of polymeric micelles, based on 16 % drug loading) were tested at 10 μg/mL, 20 μg/mL and 30 μg/mL (drug concentration in culture media). Unloaded **RGD-NanoStar** were tested at the same concentration used for testing the drug-loaded micelles: 52 μg/mL, 105 μg/mL and 158 μg/mL concentrations of polymeric micelles for 10 μg/mL, 20 μg/mL and 30 μg/mL DTX, respectively. Loaded and unloaded **RGD-NanoStar** micelles were reconstituted after lyophilization in MilliQ water for 1 mg/mL final concentration and sonicated for 5 min at 20 % Amplitude (A), while DTX free was reconstituted in DMSO for 1 mg/mL final concentration before dilution in culture media.

2.6.1. MTT assay

RGD-NanoStar micelles *in vitro* test on Ad-MSCs was performed after 24, 48 and 72 h addition to cell cultures. Cell viability assay of cancer cell lines incubated with loaded and unloaded micelles was performed at 24, 48 and 72 h of culture. At each time point, MTT assay was performed following the manufacturer's instructions. Briefly, the MTT reagent [3-(4,5-dimethylthiazol-2-yl)-2,5-diphenyltetrazolium bromide] (5 mg/mL) was dissolved in Phosphate Saline Buffer 1× (PBS 1 X) and the cells were incubated with MTT solution for 2 h at 37 °C, 5 % CO_2 and controlled humidity conditions. The media was replaced by 15 min incubation in DMSO under slight stirring conditions and the absorbance was read at 570 nm by using a Multiskan FC Microplate Photometer (Thermo Scientific). The values of absorbance are directly proportional to the number of metabolically active cells able to convert MTT reagent in a formazan-based by-product. All cell lines were seeded at a density of 15.000 cells/cm^2 in 96 well-plates. One experiment was carried out and a biological triplicate for each condition was performed.

2.6.2. Cell morphology evaluation

The morphology of cancer cell lines after 24 h of culture with **RGD-NanoStar** and **RGD-NanoStar/DTX** was evaluated at all the concentrations tested. Cells were fixed in 4 % PFA and permeabilized in PBS 1 X with 0.1 % (*v*/v) Triton X-100 (Sigma) for 5 min at room temperature, following the manufacturer's instructions. F-actin filaments were highlighted by green-fluorescent Alexa Fluor 488® phalloidin probe (Life Technologies) incubated for 20 min at room temperature. DAPI counterstaining was performed for cell nuclei identification, following the manufacturer's instructions. The images were acquired at the Inverted Ti-E Fluorescent Microscope. One experiment was carried out and a biological replicate for each condition was performed.

2.6.3. Migration analysis

RGD-NanoStar/DTX ability in inhibiting the migration of cancer cells was evaluated by performing the scratch test [35]. Cells were seeded with a density of 50.000 cells/cm^2 in 24 well-plates. Twenty-four hours after cell seeding, a p200 tip was used to do the scratch in each well and culture media was substituted with the drug and micelles diluted in scratch media consisting of basal media with 2 % FBS and 1 %

pen/strep. Cells cultured with scratch media only were used as negative control. The scratch was monitored over time and images were acquired at time 0, 24 and 30 h by using the Inverted Ti-E Fluorescent Microscope (Nikon). One experiment was carried out and a biological triplicate for each condition was performed. A representative panel of the scratch trend was proved by 4 % buffered Paraformaldehyde (PFA) fixation of cells at time 0 and 30 h followed by DAPI staining (300 nM working solution, Invitrogen) of cell nuclei.

2.6.4. Statistical analysis

Statistical analysis was performed by GraphPad Prism Software (8.0.1 version). The results of MTT assay are reported in the graphs as mean percentage of cell viability respect to cells only ± standard error of the mean and they were analyzed by Two-way analysis of variance (Two-way ANOVA) and Tukey's multiple comparisons test. For migration analysis, six measures of the scratch width were taken for each replicate at each time point by ImageJ Software; data were reported in the graphs as distance (μm) covered by cells over time from the edges towards the centre of the scratch respect to time 0 ± standard error of the mean and they were analyzed by Two-way ANOVA and Tukey's multiple comparisons test (* p value ≤0.05, ** p value ≤0.01, *** p value ≤0.001, **** p value ≤0.0001).

3. Results

3.1. Chemistry

The synthesis of *star* architectures requires a fine control over the molecular weight, the chemical composition and the number of the arms, having a significant effect on polymer properties (*e.g.* crystallinity, degradation rate, and micellization) [10,36]. Accordingly, we aim to synthesize a *star*PLA-PEG copolymer with a final molecular weight of 20.000 g/mol with a precise hydrophobic: hydrophilic ratio (*i.e.,* 14.000:6.000 g/mol) to allow the self-assembly and micellization in aqueous solution. To this end, a ROP of L-lactide monomer (**1**) using glycerol (**2**) as trifunctional alcohol initiator and DBU as organocatalyst was designed to target the three arms *star*PLA (**3**) (Scheme 1). To estimate the amount of initiator and catalyst, the degree of polymerization (DP) was calculated (see Supporting Information) starting from the desired molecular weight of the final product *star*PLA (**3**) (*i.e.,* Mn = 14.000 g/mol). Accordingly, an initial [lactide (L-LA)]$_0$/[initiator]$_0$/[DBU]$_0$ ratio of 97/1/2 ([L-LA]$_0$ = 1 M) was used. In such experimental conditions, the polymerization carried out in dichloromethane at room temperature was extremely fast, yielding almost quantitative monomer conversion (98 %) in 10 min, with easy removal of the catalyst. The reaction was quenched by addition of an excess of benzoic acid leading to DBU deactivation and (**3**) was purified by precipitation into cold methanol to avoid instability over the time due to any traces of benzoic acid/DBU salt [37]. The described method led to a very pure product with a fine control over the molecular weight and dispersity index. Moreover, a kinetic study was performed to confirm that the linear macromolecular arms grew during the ROP directly and evenly from all the three hydroxyl groups of the initiating core, in a parallel and steady manner leading to a well-defined and uniform *star*-shaped structure (see Supporting Information, Fig. S1 and S2, for details).

The terminal hydroxyl groups of (**3**) were quantitatively esterified with pentynoic anhydride (**5**), prepared from the commercial pentynoic acid (**4**), leading to a *clickable* alkynyl-terminated *star*PLA (**6**) (Scheme 1). ^{1}H NMR analysis confirmed the structure of (**6**) by the disappearance of the resonance at δ 4.36 ppm, attesting for the quantitative esterification of the terminal hydroxyl groups, together with the appearance of a novel set of signals attributed to the pentynoic end-group protons at δ 2.65, 2.52, 1.98 ppm (Supporting Information). The SEC analysis showed a dispersity value ($M_w/M_n = Đ_M$) of 1.13 and a $\bar{M}n^{SEC,app}$ = 21.207 g/mol.

In parallel, for the preparation of the hydrophilic domain of the final product, a mono-azide PEG was synthesized starting from PEG diol (**7**, Mw 2000 g/mol) in a two-step process consisting in a mono-tosylation followed by conversion of (**8**) in mono-azide PEG (**9**) by reaction with sodium azide (Scheme 2) [38]. ^{1}H NMR analysis (Supporting Information) confirmed the structure of (**9**) by the typical signal at δ 3.39 ppm relative to the azidomethylene protons. Peaks integration pointed out that the sample is a 1:1 mixture of mono-azide PEG (**9**) and unreacted PEG diol (**7**), the latter removed in the next synthetic step and related work up (see Experimental section). Moreover, the MALDI-ToF analysis (Supporting Information) excluded the presence of the undesired di-azide derivative and confirmed the azidation due to the presence of a small population showing 28 mass units less than the main population corresponding to the elimination of a nitrogen molecule during characterization typical for azide-containing polymers [39]. The alkynyl-terminated *star*PLA (**6**) and the mono-azide PEG (**9**) were then coupled in a 1:3 ratio by CuAAC reaction in the presence of CuBr and PMDETA as catalyst and ligand, respectively, to obtain the amphiphilic three-arms *star*PLA-PEG copolymer (**10**) in a very good yield (96 %) (Scheme 2). Then, the hydroxyl end-groups of (**10**) were esterified with pentynoic anhydride in presence of DMAP (Scheme 2) leading to the alkynyl terminated *star*PLA-PEG (**11**).

SEC analysis (Fig. 2A) confirmed the coupling reaction with the shift of the curve related to the *star*PLA-PEG (**10**) (red line) compared to the precursor (**6**) (blue line). The low intensity shoulder next to the main peak obtained after the CuAAC click reaction, at lower elution volume (~ 14.7 mL), indicated the presence of a negligible byproduct with a molecular weight greater than the *star*PLA-PEG (**10**). Although generally considered as highly orthogonal, the CuAAC reaction might also be subjected to certain side reactions [40], such as the Glaser coupling of the alkynyl-terminated *star*PLA (**6**) [41].

Furthermore ^{1}H NMR analysis attests for the formation of the expected triazole ring connecting the hydrophilic (PEG) and the hydrophobic (PLA) polymeric domains by the typical signal at δ 7.58 ppm (triazole H-5 proton, black circle, Fig. 2B). In addition, the shift of the

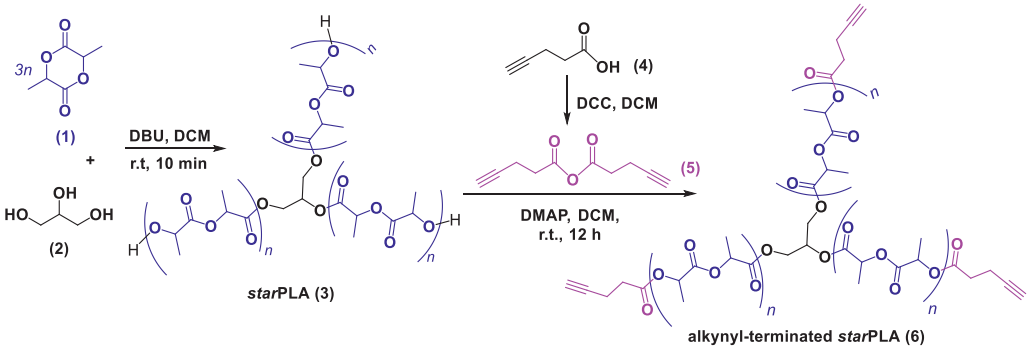

Scheme 1. Synthesis of alkynyl-terminated *star*PLA (**6**).

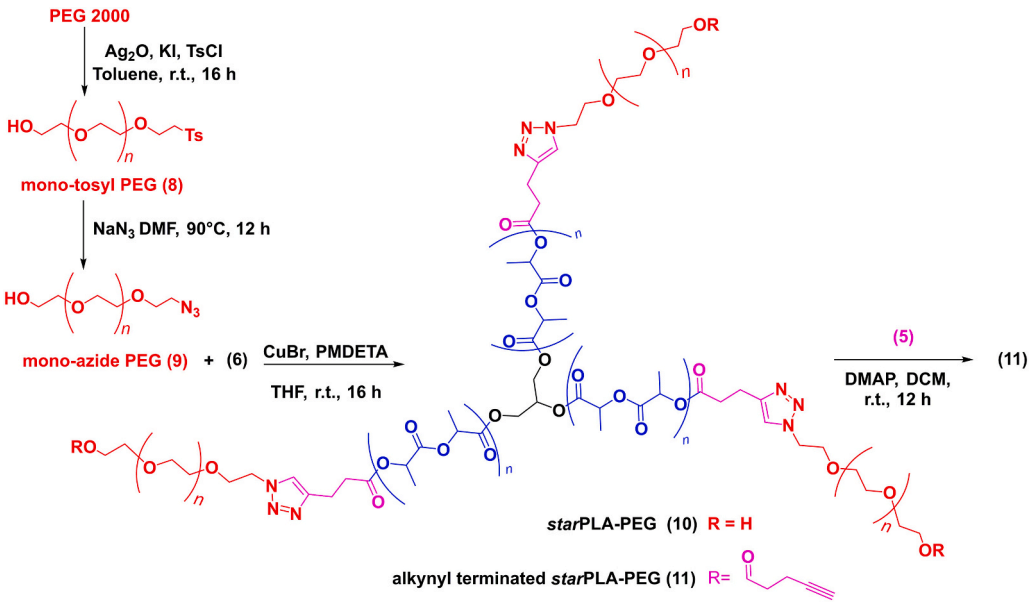

Scheme 2. Synthesis of mono-azide PEG (**9**) and subsequent CuAAC reaction with (**6**) yielding the amphiphilic *star*PLA-PEG (**10**), further functionalized to (**11**) with terminal alkynes.

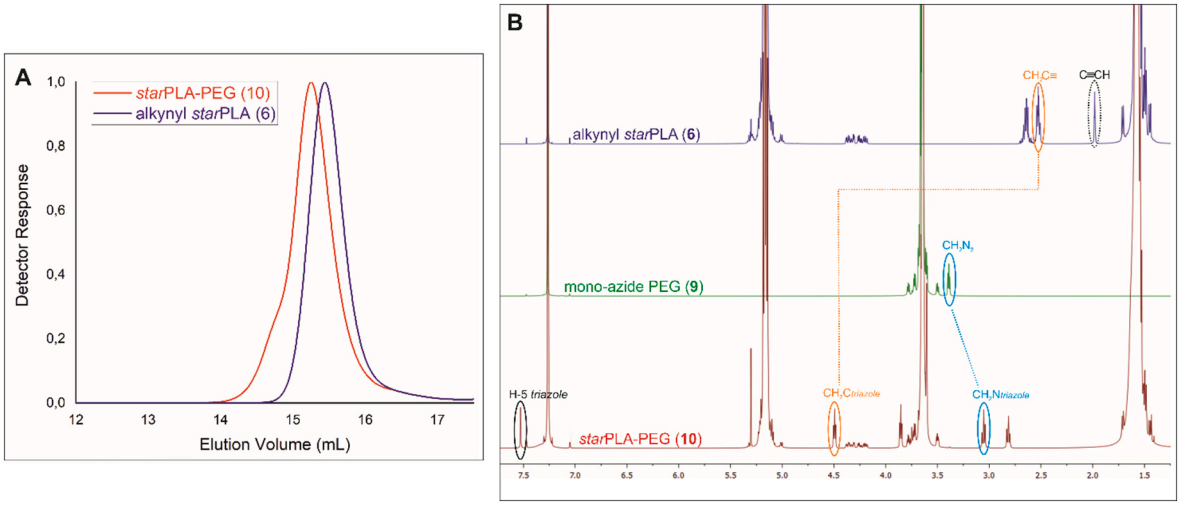

Fig. 2. A) SEC chromatograms of *star*PLA-PEG (**10**, red line) compared to alkynyl-terminated *star*PLA precursor (**6**, blue line). B) ^{1}H NMR spectra of three-arms *star*PLA-PEG (**10**, red trace), mono-azide PEG (**9**, green trace), alkynyl-terminated *star*PLA (**6**, blue trace). All the NMR spectra were recorded in $CDCl_3$ at r.t. (For interpretation of the references to colour in this figure legend, the reader is referred to the web version of this article.)

azido-methylene protons resonance (from δ 3.39 to 3.06 ppm, blue circles), the shift of the pentynoic-methylene protons signal (from δ 2.52 to 4.49 ppm, orange circles), together with the disappearance of the alkyne proton signal at δ 1.98 ppm were observed (black dashed circle, Fig. 2B).

Arg-Gly-Asp (RGD) peptide sequence has been identified as a useful tumor targeting ligand to selectively recognize $\alpha_v\beta_3$ integrin. [17] Moreover, it was found that cyclic RGD pentapeptides not only have

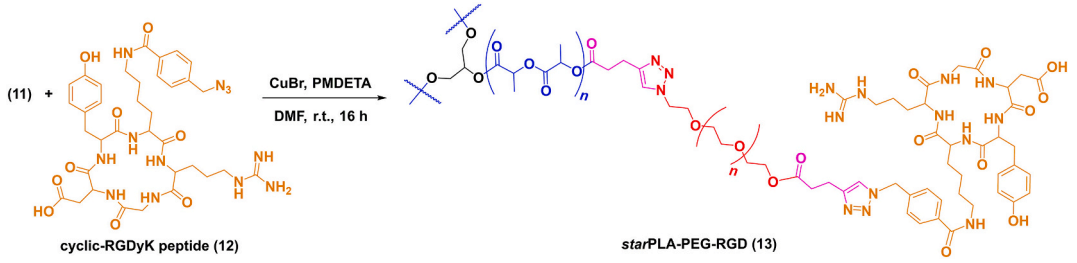

Scheme 3. Decoration of alkynyl-terminated *star*PLA-PEG (**11**) with azido cyclic-RGDyK peptide (**12**) leading to the target three-arms RGD-decorated *star*PLA-PEG (**13**).

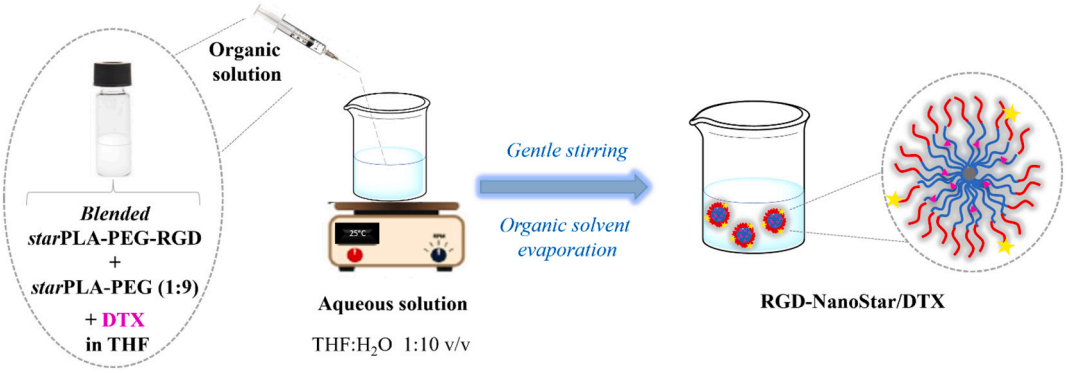

Fig. 3. Schematic representation of the nanoformulation of **RGD-NanoStar/DTX**.

high affinity to $\alpha_v\beta_3$, but also exhibit high metabolic stability *in vivo*, [42] a crucial prerequisite for successful *in vivo* application. Therefore, the final decoration of the alkynyl-terminated *star*PLA-PEG (**11**) with azido cyclic-RGDyK peptide (**12**, Arg-Gly-Asp-D-Tyr-Lys) was carried out by CuAAC reaction (Scheme 3) and the structure of (**13**) was confirmed by ^{1}H NMR analysis (Supporting Information) by the characteristic signals (δ 7.96, 7.43, 7.02, 6.72 ppm) ascribable to aromatic protons of both Tyr and benzamide moieties of RGD, together with several broad peaks likely related to NH-protons (from δ 8.74 to δ 7.61 ppm). The integration of the peak at δ 7.43 ppm of RGD compared to those of the PLA block (δ 5.28 ppm), used as a reference, revealed that the PLA block remained almost intact during the reaction and a coupling efficiency of 50 % was obtained. Furthermore, SEC analysis carried out by connecting in parallel a differential refractometer detector and a UV–Vis spectrophotometer set at the λ_{max} of RGD (*i.e.,* 280 nm) confirmed the grafting of RGD on the polymer backbone (data not shown).

The decoration of the *star*PLA-PEG backbone with RGD peptide did not alter the molar mass of the polymer as the RGD contribution is neglectable (RGD MW 892 Da) respect to the molecular weight of the whole polymer but strongly influenced the amphiphilic properties and the related self-assembly behavior, as suggested by the peculiar SEC profile and DLS measurements in THF (Supporting Information). Specifically, SEC analysis of *star*PLA-PEG-RGD showed a main distribution centered at 15.5 mL and a minor one likely obtained by partial aggregation of these *star*-based structures. This behavior was also confirmed by DLS measurements showing a bimodal size distribution in the same solvent (*i.e.*, THF) with the presence of two species having a D_H of about 10 and 100 nm; the small one might be related to the unimolecular micelles, whereas the large one should come from the self-assembled multi-micelle aggregates.

3.2. Preparation and characterization of starPLA-PEG-RGD micelles

The nanoformulation of *star*PLA-PEG-RGD (**13**) and the drug encapsulation into the polymeric micelles were carried out by nanoprecipitation (Fig. 3) at two different polymer: drug ratios (*i.e.,* 10:1 and a 10:3). The *star*PLA-PEG-RGD was nanoformulated in the presence of *star*PLA-PEG precursor in a 1:9 binary blend [42]. Briefly, blended polymer and DTX were dissolved in THF and added dropwise into an aqueous solution under stirring. The micelles formed during the rapid diffusion of the organic solution in the non-solvent. After THF removal, the colloidal solution was gently centrifuged to remove the unloaded free drug insoluble in water and the supernatant was freeze-dried to obtain **RGD-NanoStar/DTX**. Empty micelles (**RGD-NanoStar**) were prepared following the same procedure, without adding the drug.

The drug loading (DL) measured by UV–Vis spectrophotometry resulted 16 % and 6 % for the 10:3 and 10:1 formulations, respectively; the encapsulation efficiency (EE) was estimated to be 69 % and 57 %, respectively (Table 1). The mean hydrodynamic diameter (D_H) of **RGD-NanoStar/DTX** resulted 283 ± 50 nm and 379 ± 138 nm for the 10:3 and 10:1 nanoformulations, respectively (Table 1), with a second population at 70 ± 9 nm and 129 ± 29 nm which is negligible (8 %) for the 10:3 formulation and more evident (44 %) for the 10:1. Based on all these findings, the 10:3 nanoformulation was selected for the biological investigation. The unloaded **RGD-NanoStar** owned a monomodal particle size distribution (133 ± 51 nm) before centrifugation and freeze-drying (freshly prepared), whereas the D_H value slightly increased after lyophilization and reconstitution (Table 1). The zeta potential attested for negatively charged micelles, with a net negative charge ranging from −25 to −20 mV which is rather common for aliphatic polyester nanoparticles indicating good colloidal stability. This negative surface charge can be likely ascribed to a preferential adsorption or

Table 1
Overall Properties of micelles: mean Hydrodynamic Diameter (D_H), PDI and zeta potential (ζ) in Ultrapure Water;[a] Theoretical Loading (TL), Drug Loading (DL) and Encapsulation Efficiency (EE). Size Distributions and ζ-Potential are reported in Fig. S3, Supporting Information.

Sample	D_H (nm ± SD) (%)[b]	PDI	ζ (mV ± SD)	TL (%)	DL (%)[c]	EE (%)[d]
RGD-NanoStar/DTX (10:3) (Lyophilized and reconstituted)	283 ± 50 (92 %) 70 ± 9 (8 %)	≅ 0.3 ≅ 0.2	−22 ± 4	23	16	69
RGD-NanoStar/DTX (10:1) (Lyophilized and reconstituted)	379 ± 138(56 %) 129 ± 29 (44 %)	≥0.4 ≅ 0.4	−25 ± 4	9	6	57
RGD-NanoStar (Lyophilized and reconstituted)	259 ± 76 (93 %) 55 ± 6 (7 %)	≥0.4 ≅ 0.2	−20 ± 4	–	–	–
RGD-NanoStar (Freshly prepared)	133 ± 51	≥0.4	−22 ± 7	–	–	–

[a] Each DLS and ζ-Potential measurement was carried out in triplicate, at 25 °C (SD was calculated on the three different batches).
[b] Size with corresponding intensity % distribution.
[c] Actual loading is expressed as the amount of drug (mg) encapsulated per 100 mg of nanoparticles.
[d] Ratio between actual (DL) and theoretical (TL) loading × 100.

binding of hydroxyl anions (originated by water autodissociation) to the oligo(ethylene glycol) chains of the *star* polymer at the interface between the PEGylated nanoparticles and the bulk aqueous solution [43–45]. However, the decoration of nanoparticles surface with the RGD peptide did not significantly affect the zeta potential values in well agreement with analogous RGD-decorated PLGA-PEG nanoparticles exhibiting rather high negative zeta potential values in deionized water with or without peptide. [46].

To investigate the stability of our **RGD-NanoStar/DTX** and the influence of the dispersing medium on the aggregation of our nanosystem, stability studies were carried out *vs.* time in ultrapure water and in biologically relevant medium, such as PBS (pH 7.4). The size distribution of the nanosystem was monitored by DLS, remaining approximately constant within 7 days. Moreover, **RGD-NanoStar/DTX** showed a fairly stable zeta potential in ultrapure water within 7 days.

The CMC of the micelles, calculated by fluorescence spectrophotometry using pyrene as a probe, was 0.01 mg/mL for both *star*PLA-PEG and *star*PLA-PEG-RGD.

Star polymers, given their small dimensions, are challenging to observe *via* direct imaging using microscopy techniques such as atomic force microscopy (AFM) and transmission or scanning electron microscopy (TEM/SEM) as they are often below the resolution limits or collapsed into globular structures (see Supporting Information), obscuring the fine structural detail of these architecturally complex macromolecules [2].

The release performance of drug-loaded nanoparticles is an important index to evaluate performance and effectiveness. Accordingly, release experiments have been carried out in PBS (pH 7.4) at 37 °C using the dialysis method (Supporting Information). Based on our experimental results, it is possible to admit that the drug released from **RGD-NanoStar/DTX** within 1 week (~58 %, corresponding to 192.2 μg DTX) remained substantially entrapped into the dialysis membrane along the time, likely due to the high lipophilicity of the drug and its poor solubility in the buffer solution despite the addition of Tween 80. Therefore, it was not possible to obtain a typical release curve, rather we determined the overall amount of DTX released from **RGD-NanoStar/DTX** within 1 week. Moreover, the incomplete release after 7 days might be related to a strong interaction between the drug and polymer and a slow degradation of the polymer matrix, since the release of drug from polymeric nanoparticles is a complex process mainly associated with the polymer degradation/erosion as well as with the drug diffusion and strictly related to the constituents and architectures of copolymers and to the physicochemical properties of the drug [47].

3.3. Biology

3.3.1. Evaluation of RGD-NanoStar cytotoxicity

To exclude a potential cytotoxic effect of **RGD-NanoStar**, human Ad-MSCs were selected as healthy cell model and the cell viability of treated cells was analyzed by MTT assay after 24, 48 and 72 h of culture with three different concentrations (*i.e.,* 52 μg/mL; 105 μg/mL; 158 μg/mL), namely the same concentrations used to test the anticancer effect of **RGD-NanoStar/DTX**. The results showed no statistically significant differences in Ad-MSCs cell viability at any time points and at any concentration tested, demonstrating the absolute absence of toxicity of **RGD-NanoStar** on healthy cells (Fig. 4).

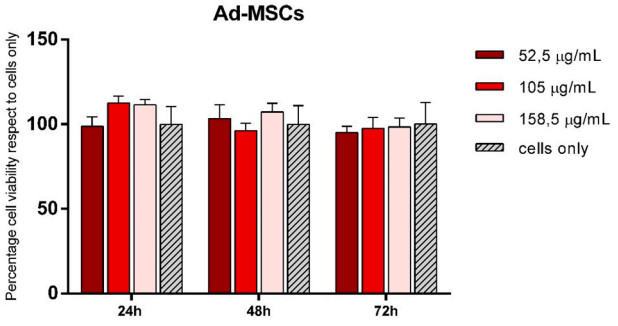

Fig. 4. Cell viability of Ad-MSCs. MTT assay on human Ad-MSCs after 24, 48 and 72 h of culture with different concentrations of **RGD-NanoStar**.

3.3.2. Evaluation of anticancer effect of RGD-NanoStar/DTX

The potential anticancer effect of **RGD-NanoStar/DTX** was tested on U87 and MDA-MB 468 tumoral cell lines at 24, 48 and 72 h of culture with three different concentrations (*i.e.,* 10 μg/mL DTX content and 52 μg/mL **RGD-NanoStar** content; 20 μg/mL DTX content and 105 μg/mL **RGD-NanoStar** content; 30 μg/mL DTX content and 158 μg/mL **RGD-NanoStar** content). Looking in detail at the trend of the results (Figs. 5 and 6), free DTX was significantly cytotoxic compared to cells only, as expected (γ: p value ≤0.01, p value ≤0.001 and p value ≤0.0001 at 10, 20 and 30 μg/mL, respectively, for U87 cells at 24 h; p value ≤0.01 and p value ≤0.0001 at 10, 20 and 30 μg/mL, respectively, for MDA-MB 468 cells at 24 h; p value ≤0.0001 at all tested concentrations for both cell lines at 48 and 72 h).

Overall, a significant reduction of cell viability in the presence of **RGD-NanoStar/DTX** was observed for both cancer cell lines, at all the time points of the experiment (Figs. 5 and 6). However, the cytotoxic effect of DTX seems to be hidden when the drug is loaded on micelles in both the cell lines. In detail, 20 and 30 μg/mL of free DTX showed higher activity compared to the same concentration loaded on micelles in U87 cell line at 48 and 72 h (p value ≤0.0001 for 30 μg/mL at 48 h and p value ≤0.01 and p value ≤0.001 for 20 and 30 μg/mL, respectively, at 72 h) (Fig. 5, H, F, and I).

Unexpectedly, a relevant anticancer effect was exerted by unloaded **RGD-NanoStar** starting from 48 h of culture, especially on MDA-MB 468 cells (Fig. 6). Indeed, while at 24 h the free drug activity is higher compared to drug-loaded and unloaded micelles (p value ≤0.05 and p value ≤0.01 for 20 and 30 μg/mL, respectively, for both drug-loaded and unloaded micelles), **RGD-NanoStar** exerted the same cytotoxicity of free DTX and of **RGD-NanoStar/DTX** at 48 and 72 h with about 40 % and 60 % of dead cells, respectively, at all tested concentrations (Fig. 6, B, C, E, F, H, I). A time-depended trend of cytotoxicity was evident on MDA-MB 468 cells, where a statistically significant difference in the presence of both **RGD-NanoStar** and **RGD-NanoStar/DTX** was observed at all tested concentrations over the time (p value ≤0.001 for 20 and 30 μg/mL **RGD-NanoStar/DTX** and for the highest concentration of **RGD-NanoStar** at 48 h; p value ≤0.01 for 10 μg/mL **RGD-NanoStar/DTX** and for 52 and 105 μg/mL of **RGD-NanoStar** at 48 h; p value ≤0.0001 for both drug-loaded and unloaded micelles at all tested concentration at 72 h) (Fig. S4, E and F).

According to Ad-MSCs results, **RGD-NanoStar** were not particularly toxic against U87 cells at 24 and 48 h (Fig. 5, A and B), but, surprisingly, they significantly reduced the cell viability of such cell line, compared to cells only, at 72 h (p value ≤0.05 and p value ≤0.01 for 52 μg/mL and, 105 and 158 μg/mL concentrations, respectively) (Fig. 5, C, F, I). The analysis of these data also demonstrated a time-dependent anticancer effect by the highest concentrations of unloaded **RGD-NanoStar** (105 and 158 μg/mL) inducing a significant decreasing in cell viability between 24 and 72 h on U87 cells (p value ≤0.01 for both concentrations) (Fig. S4, C).

3.3.3. Cell morphology evaluation

A qualitative cell morphology evaluation was performed on both the cancer cell lines after 24 h of culture with free DTX, **RGD-NanoStar/DTX** and unloaded **RGD-NanoStar,** compared to cells only. The fluorescent analysis confirmed the previously reported cell viability data. Overall, a compromised cell morphology was observed in the presence of both free DTX and **RGD-NanoStar/DTX** (Fig. 7). Specifically, a high presence of round-shape morphology in both cell lines was observed at the highest concentrations (Fig. 7, panel 1 and 2, images D and G)

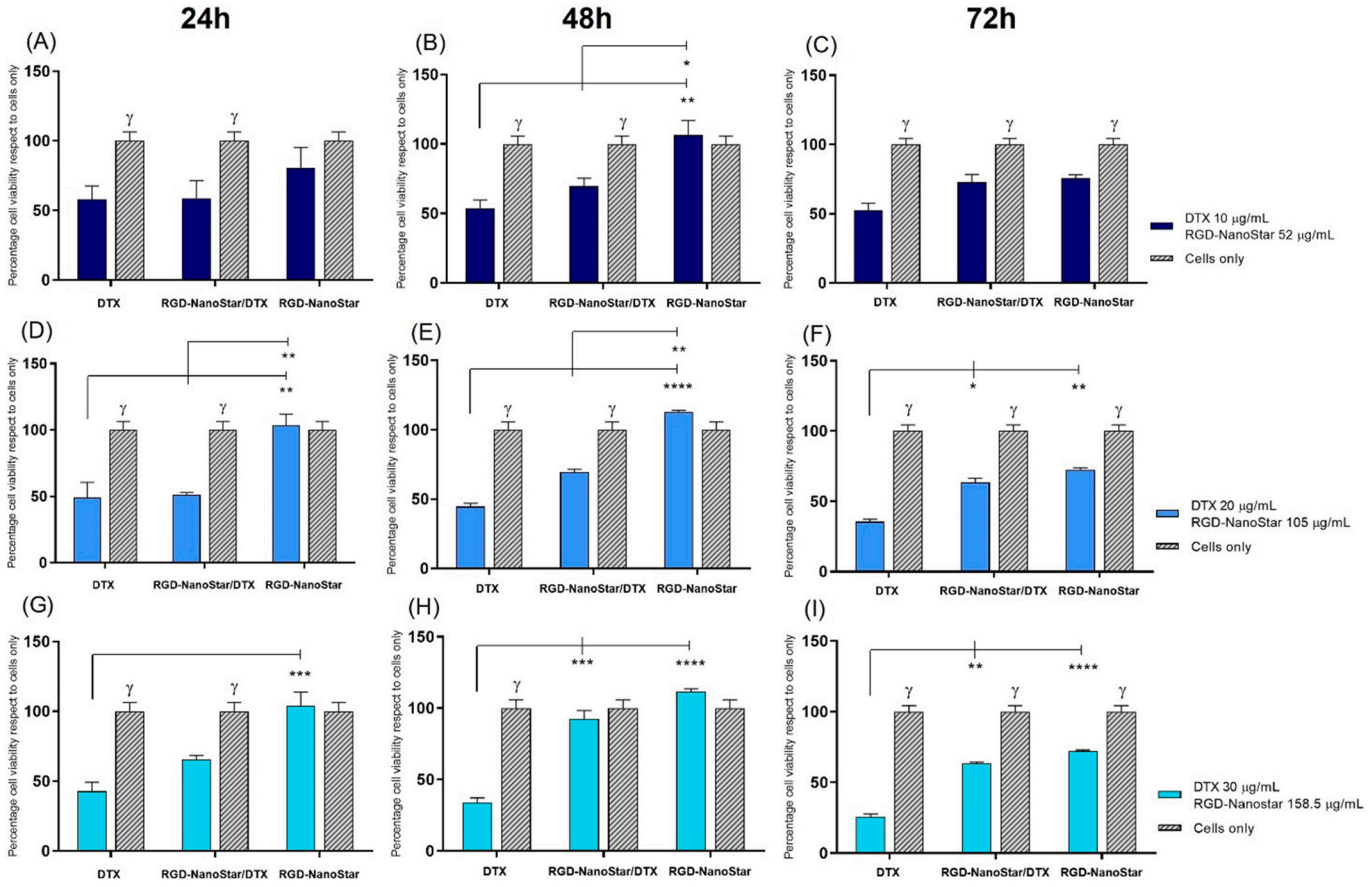

Fig. 5. Anticancer effect of **RGD-NanoStar/DTX** on U87 cell line. MTT assay on U87 after 24 (A, D and G), 48 (B, E and H) and 72 h (C, F and I) of culture with free DTX, unloaded **RGD-NanoStar** and drug-loaded **RGD-NanoStar/DTX** at 10 μg/mL (A, B and C), 20 μg/mL (D, E and F) and 30 μg/mL (G, H and I) concentrations. Statistically significant differences of DTX, **RGD-NanoStar/DTX** and **RGD-NanoStar** compared to cells only are graphically represented by γ symbol: A) *p* value ≤0.01 and *p* value ≤0.05 for DTX and **RGD-NanoStar/DTX**; B) *p* value ≤0.001 and *p* value ≤0.05 for DTX and **RGD-NanoStar/DTX**; C) *p* value ≤0.0001, *p* value ≤0.01 and *p* value ≤0.05 for DTX, **RGD-NanoStar/DTX** and **RGD-NanoStar**, respectively; D) *p* value ≤0.001 and *p* value ≤0.01 for DTX and **RGD-NanoStar/DTX**; E) *p* value ≤0.0001 and *p* value ≤0.05 for DTX and **RGD-NanoStar/DTX**; F) *p* value ≤0.0001, *p* value ≤0.001 and *p* value ≤0.01 for DTX, **RGD-NanoStar/DTX** and **RGD-NanoStar**, respectively; G) *p* value ≤0.0001 and *p* value ≤0.05 for DTX and **RGD-NanoStar/DTX**; H) *p* value ≤0.0001 for DTX; I) *p* value ≤0.0001, *p* value ≤0.001 and *p* value ≤0.01 for DTX, **RGD-NanoStar/DTX** and **RGD-NanoStar**, respectively. Statistically significant differences among samples are graphically represented (* *p* value ≤0.05, ** *p* value ≤0.01, *** *p* value ≤0.001, **** *p* value ≤0.0001).

without significant difference in cell morphology between DTX- and **RGD-NanoStar/DTX** – treated cells, especially in U87 cell line. The absence of cytotoxicity by unloaded **RGD-NanoStar** in both cell lines at 24 h was confirmed, however a slight decrease in cell number was observed in the presence of **RGD-NanoStar** for both cell lines compared to cells only, validating the previously reported long-term anticancer effect produced by unloaded micelles in later times (Fig. 7, panel 1 and 2, images C, F, I and L).

3.3.4. Inhibition of cell migration induced by RGD-NanoStar/DTX

The role of **RGD-NanoStar/DTX** in inhibiting the migration of cancer cells was investigated by scratch test analysing the distance (μm) covered by cells over time towards the centre of a scratch performed at time 0 in the well [35]. Overall, a statistically significant inhibition of cell migration was observed by all the tested concentrations of free DTX and **RGD-NanoStar/DTX** on both tumoral cell lines starting from 24 h compared to cells only (all *p* value ≤0.0001 at both 24 and 30 h, marked by Φ symbol) (Fig. 8), as evidenced by the representative panels of DAPI staining (Fig. 9) highlighting the absence of difference in scratch width over time for both cell lines. The overall total absence of statistically significant results in covered distance attested for the same inhibitory activity exerted by free DTX and **RGD-NanoStar/DTX** over time (Fig. 8). However, looking in detail, 10 and 30 μg/mL of **RGD-NanoStar/DTX** surprisingly showed higher inhibition of migration in MDA-MB 468 and U87 cell lines, respectively, compared to free drug (Fig. 8, C and D). Indeed, only 43 μm distance was covered by U87 cells after 30 h of culture with 30 μg/mL of **RGD-NanoStar/DTX** compared to 73 μm in the presence of DTX free (Fig. 8, C). More relevant, a significant difference in migration inhibition was showed in MDA-MB 468 cells, where a totally absence of cell movements was detected in the presence of **RGD-NanoStar/DTX** at 10 μg/mL compared to about 50 μm distance covered by cells in the presence of free DTX at 30 h (*p* value ≤0.0001) (Fig. 8, D).

4. Discussion

Here, a novel amphiphilic copolymer based on three armed *star*PLA-PEG was synthesized with predicted molecular weight and well-designed hydrophobic:hydrophilic ratio in a typical *core-first* approach by a combination of ROP and *click* chemistry. The *star* copolymer was eventually decorated with the tumor-targeting ligand cyclic-RGDyK peptide for drug delivery purposes. The final compound and molecular sub-units in each synthetic step were fully characterized by NMR, SEC, and MALDI-ToF analysis, pointing out a fine control of the polymer architecture through the multi-step synthesis in terms of polymerization degree, molecular weight and molecular weight distribution. The anticancer drug DTX was efficiently loaded into **RGD-NanoStar** micelles with a good encapsulation efficiency (69 %) by the well-established

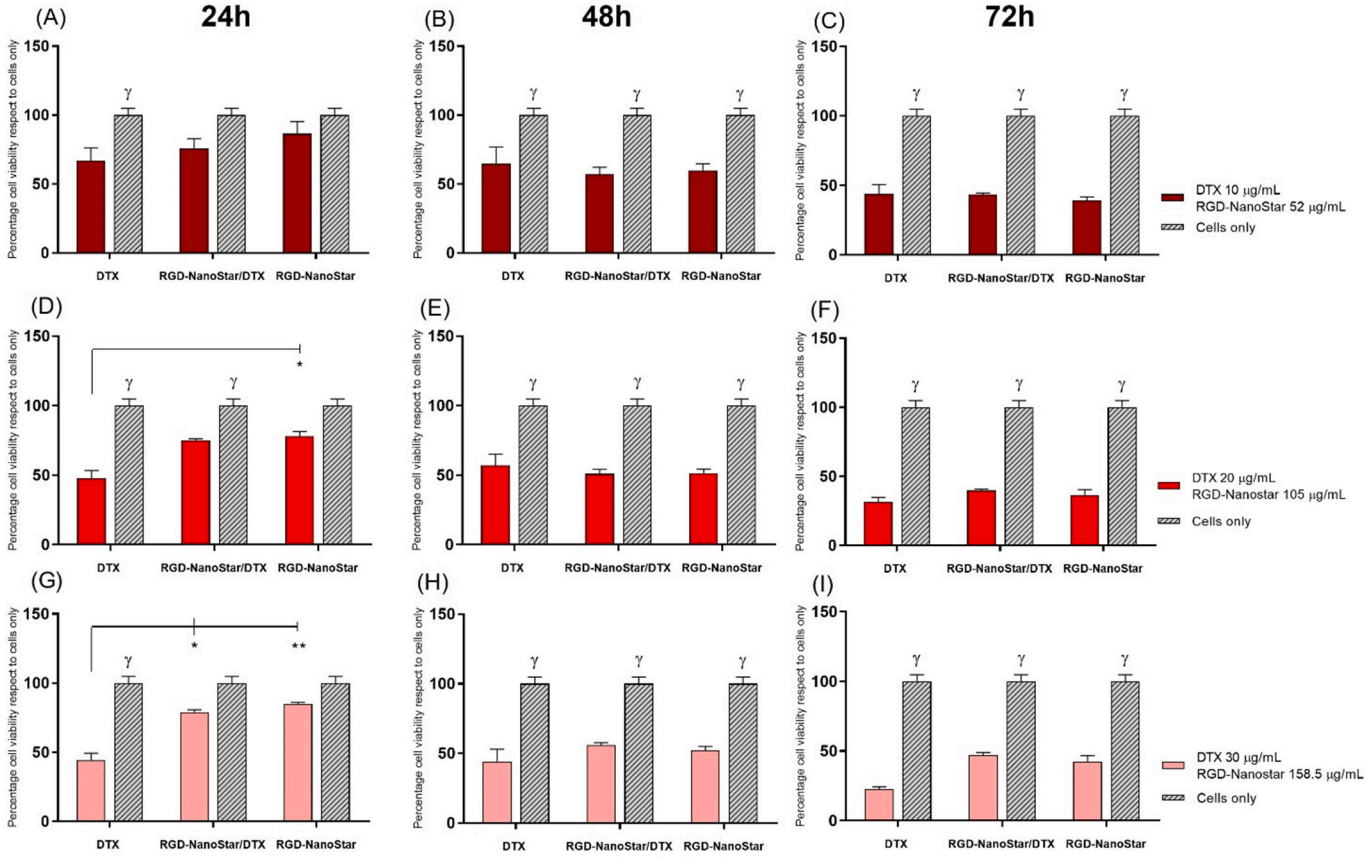

Fig. 6. Anticancer effect of **RGD-NanoStar/DTX** on MDA-MB 468 cell line. MTT assay on MDA-MB 468 after 24 (A, D and G), 48 (B, E and H) and 72 h (C, F and I) of culture with free DTX, unloaded **RGD-NanoStar** and drug-loaded **RGD-NanoStar/DTX** at 10 μg/mL (A, B and C), 20 μg/mL (D, E and F) and 30 μg/mL (G, H and I) concentrations. Statistically significant differences of DTX, **RGD-NanoStar/DTX** and **RGD-NanoStar** compared to cells only are graphically represented by γ symbol: A) *p* value ≤0.01 for DTX; B) *p* value ≤0.01 and *p* value ≤0.001 for DTX and **RGD-NanoStar**, and **RGD-NanoStar/DTX**, respectively; C) *p* value ≤0.0001 for all samples; D) *p* value ≤0.0001 and *p* value ≤0.05 for DTX and **RGD-NanoStar/DTX**; E, F) *p* value ≤0.0001 for all samples; G) *p* value ≤0.0001 for DTX; H) *p* value ≤0.0001 and for *p* value ≤0.001 DTX and **RGD-NanoStar**, and **RGD-NanoStar/DTX**, respectively; I) *p* value ≤0.0001 for all samples. Statistically significant differences among samples are graphically represented (* *p* value ≤0.05, ** *p* value ≤0.01, *** *p* value ≤0.001, **** *p* value ≤0.0001).

nanoprecipitation method using a 10:3 polymer to drug ratio. Typically, a polymer solution in THF containing the drug was mixed with an excess amount of a miscible relatively poor solvent (water) to induce the spontaneous nanoparticle formation, as confirmed by DLS analysis. As expected, drug-loaded **RGD-NanoStar/DTX** showed a greater D_H compared to unloaded **RGD-NanoStar** (283 ± 50 *vs* 259 ± 76 nm, measured on lyophilized and reconstituted samples) likely due to the typical *core-shell* structure promoting hydrophobic interactions between the PLA *core* and the hydrophobic drug which favor DTX to be trapped into the inner *core*, leading to size changes. As well known, unimolecular micelles can self-assemble in a kind of multi-micelle aggregates characterized by the entanglement of the hydrophilic branches, and/or they can rearrange forming primary micelles, where the hydrophilic arms stabilize an aggregate of hydrophobic cores [48]. The observed D_H values attested for micellar aggregates. Specifically, the entanglement of the hydrophilic branches of our *star* polymer, favored by the flexibility of the PEG chain, formed a dense network structure, with D_H values ranging from 133 to 283 nm for the best nanoformulations. Moreover, a negligible peak was observed by DLS at 0.3 mg/mL (above the CMC of 0.01 mg/mL) for both **RGD-NanoStar/DTX** and **RGD-NanoStar** at 70 ± 9 nm and 55 ± 6 nm (8 and 7 %, intensity distribution), respectively. The coexistence of the two species, and specifically, the formation of unimolecular micelles in equilibrium with larger associated micelles has been reported in several papers [49–50], where the hundred-nanometer-sized species were multi-micelle aggregates built up from the aggregation of unimolecular micelles, whereas the smallest species were considered the unimolecular micelles. Interestingly, the freshly prepared **RGD-NanoStar/DTX**, analyzed before centrifugation and freeze-drying, owned a monomodal particle size distribution (133 ± 51 nm). Moreover, the slightly increased D_H (259 ± 76 nm) and the appearance of a negligible peak at 55 ± 6 nm (7 %), observed after lyophilization and reconstitution, pointed out a slight agglomeration occurring during those stages and the coexistence of the two populations was plausibly ascribed to the formation of smaller aggregates of unimolecular micelles in equilibrium with larger associated micelles. The zeta potential value attested for negatively charged micelles and showed less variability between loaded and unloaded micelles, confirming that the filling of the *core* did not change the surface charge.

The biological profile of the unloaded **RGD-NanoStar** was firstly investigated on human primary Ad-MSCs to exclude a potential cytotoxic effect on healthy cells, and a total absence of toxicity was found on Ad-MSCs at any concentration and time points tested (Fig. 4). Surprisingly, an important time-dependent reduction of cell viability, comparable as both the free DTX and **RGD-NanoStar/DTX**, was exerted by unloaded **RGD-NanoStar** on MDA-MB 468 breast cancer cells, starting from 48 h of culture (about 40 % and 60 % of dead cells at 48 and 72 h, respectively, at all tested concentrations, Figs. 5 and 6). Moreover, **RGD-NanoStar** reduced the cell viability also of brain tumor U87 cells, compared to cells only, at 72 h (about 30 % of dead cells), demonstrating a time-dependent effect exerted by the highest concentrations (105 and 158 μg/mL) (Figs. 5 and 6).

It was already demonstrated that RGD-targeted polymeric micelles

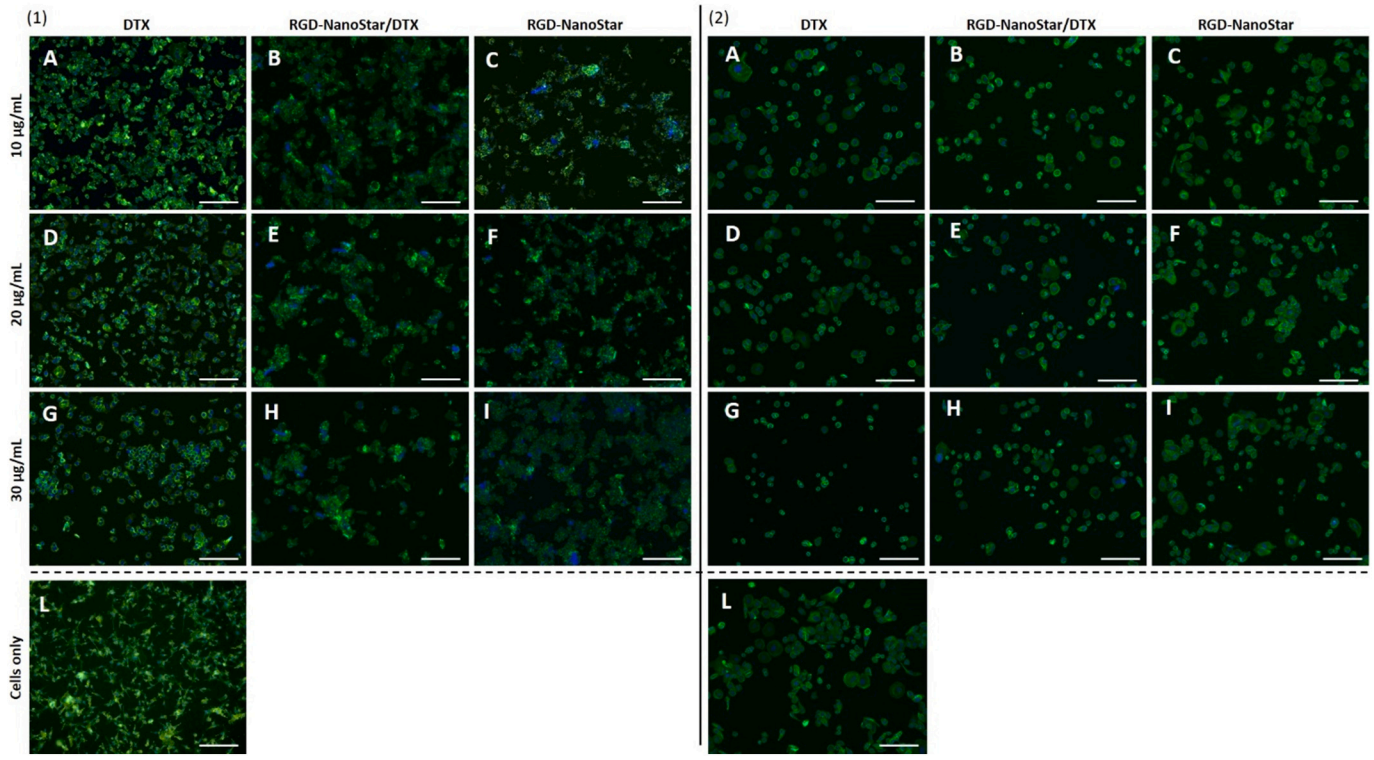

Fig. 7. Actin and DAPI staining. Cell morphology evaluation of U87 (panel 1) and MDA-MB 468 cells (panel 2) in the presence of different concentrations of free DTX (images A, D, and G), **RGD-NanoStar/DTX** (images B, E and H) and **RGD-NanoStar** (images C, F and I) compared to cells only (images L). Green-fluorescent phalloidin probe and DAPI counterstaining were performed on cancer cell lines; F-actin filaments in green, cell nuclei in blue. Scale bars 200 µm. (For interpretation of the references to colour in this figure legend, the reader is referred to the web version of this article.)

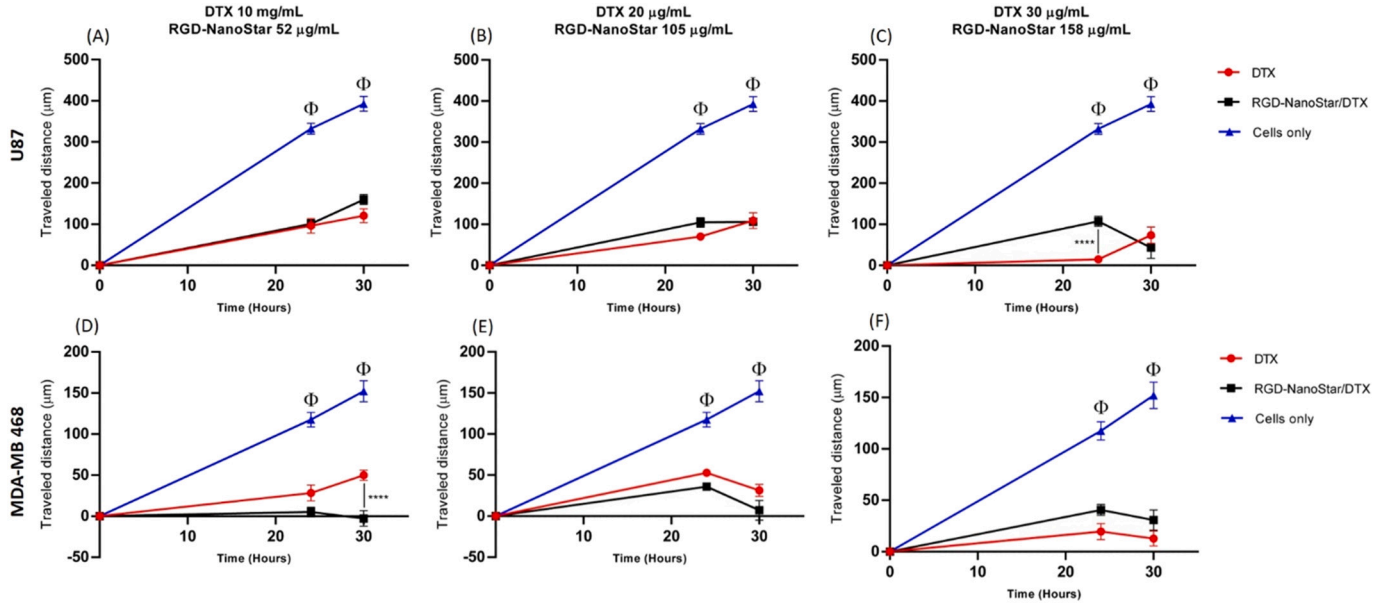

Fig. 8. Migration inhibition of cancer cell lines. Scratch test on U87 (A, B and C) and MDA-MB 468 (D, E and F) cultured with free DTX and **RGD-NanoStar/DTX**. Statistically significant differences of covered distance in the presence of free DTX and **RGD-NanoStar/DTX** respect to cells only are graphically represented by Φ symbol as p value $\leq$0.0001 at both 24 and 30 h for all concentrations. Statistically significant differences between the samples at the same concentration are reported in the graphs (**** p value $\leq$0.0001).

improved cancer cells internalization and toxicity [51]. We could speculate that the well-known alteration of cancer cells metabolic pathways [52], together with the active role of the RGD motif in the cellular uptake [53], could synergistically increase the interaction of cancer cells with our micelles leading to a higher level of cytotoxicity. These biological results have been considered a significant starting point for the development of a successful delivery system which does not compromise the behavior of non-cancer cells owning specific interaction and toxicity towards cancer cells, primarily MDA-MB 468 cell line, that could be exploited for a perspective design of target therapy.

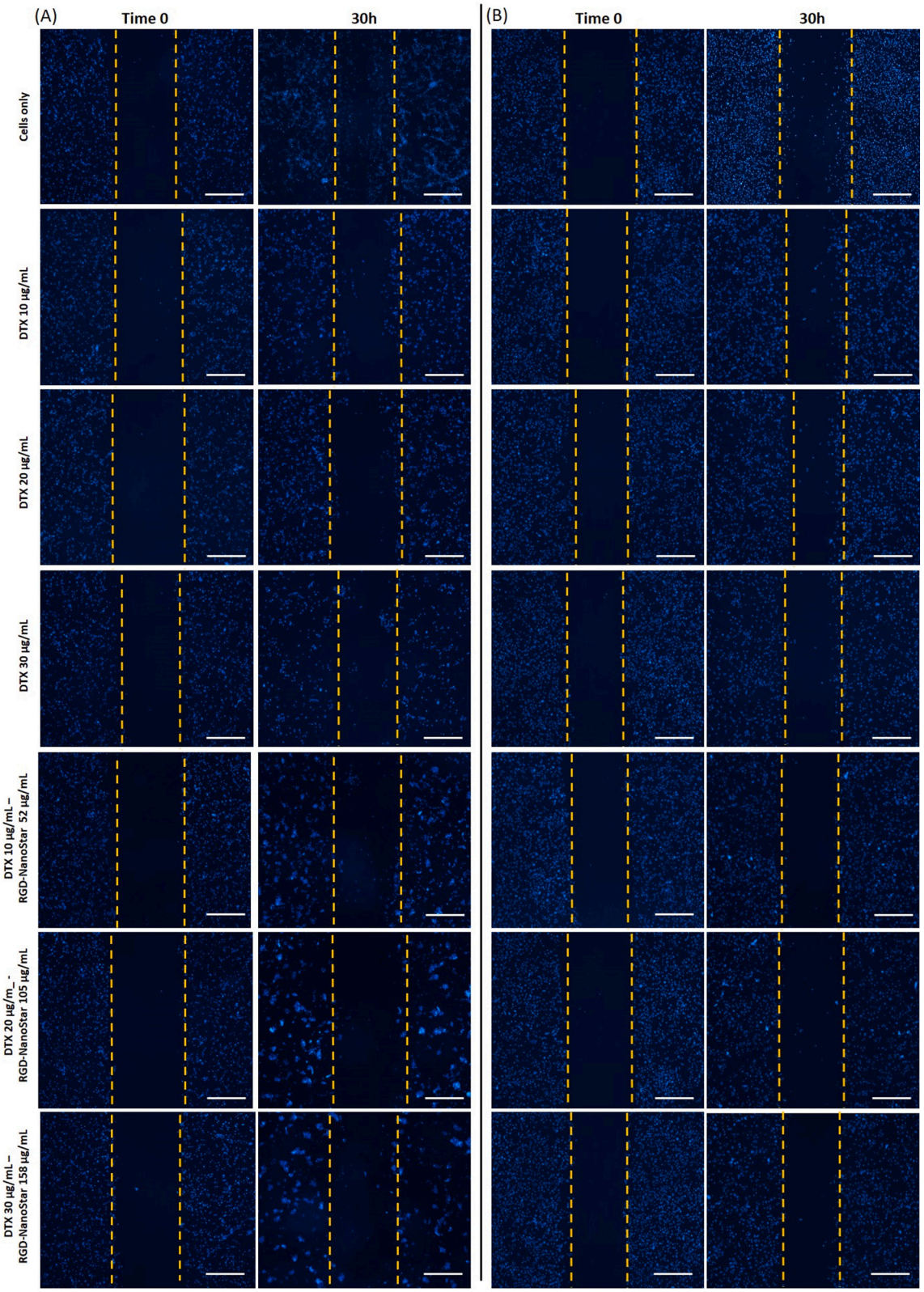

Fig. 9. Scratch test. DAPI staining of cell nuclei of U87 (panel A) and MDA-MB 468 cells (panel B) at time 0 and after 30 h of culture with free DTX and **RGD-NanoStar/DTX**. The panels highlight the absence of cell migration towards the centre of the scratch in the presence of **RGD-NanoStar/DTX** and free DTX, compared to cells only. Cell nuclei in blue. Scale bars 500 µm. One representative image for each experimental condition was reported. (For interpretation of the references to colour in this figure legend, the reader is referred to the web version of this article.)

Overall, a significant reduction of cell viability was observed on both tumoral U87 and MDA-MB 468 cells treated with **RGD-NanoStar/DTX** at all the time points (Fig. 5) together with a compromised cell morphology (Fig. 6), although the cytotoxic effect of DTX seems to be hidden when the drug is loaded on micelles. These findings can be expected owing to the high stability (the density of PEG on the *star* micellar surface provided high steric stabilization) and consequent gradual release dynamics of the drug molecule from micelles, typical of such delivery systems, preventing burst release of DTX and minimizing, in perspective, drug loss and systemic toxicity [54]. Specifically, differently from the free drug which easily diffuses into the cell, micellar drugs have to be released from the nanoparticles prior to exhibiting any therapeutic action. In this regards, **RGD-NanoStar/DTX** could gradually and sustainably release the drug, providing a continuous supply of DTX and a prolonged action over an extended period not observable at the incubation time of MTT assay. The MTT results indicated that DTX loaded into the nanosystem induced on tumoral cells anticancer effects similar to that of free DTX, especially on MDA-MB 468 breast cancer cells. Although no apparent benefit emerged from DTX incorporation into the nanosystem with respect to the free drug by evaluating the cellular viability, promising results were revealed by the analysis of the role of **RGD-NanoStar/DTX** in inhibiting the migration of cancer cells (Figs. 7 and 8). A marked migration ability is a well-recognized property of tumoral cells, which is pivotal for tumor propagation and invasiveness, giving rise to metastasis [24]. DTX is a well-known already used drug in clinics to be involved in the inhibition of such cell behavior [24–26]. The scratch assay was carried out to analyse the distance (in μm) covered by cells over time towards the centre of a scratch performed in the well. The scratch was done at time 0 in a cell culture and the cells movements were monitored over the time (for a total of 30 h of culture) under a microscope to observe the cellular migratory ability [35]. A statistically significant inhibition of tumoral cell migration was exerted by all the tested concentrations of free DTX and **RGD-NanoStar/DTX** on both the cell lines starting from 24 h, compared to cells only (Fig. 7), confirming the well-known role of DTX in inhibiting cell movements even when loaded on polymeric micelles. Surprisingly, **RGD-NanoStar/DTX** exerted higher inhibition of migration of MDA-MB 468 and U87 cell lines compared to free DTX at 10 and 30 μg/mL, respectively. Specifically, only 43 μm distance was covered by U87 cells after 30 h exposure on **RGD-NanoStar/DTX** compared to 73 μm in the presence of free DTX at the same concentration (30 μg/mL). More interestingly, a total absence of MDA-MB 468 breast cancer cell movements was detected at 30 h compared to about 50 μm distance covered by cells in the presence of free DTX at 10 μg/mL. The stronger inhibitory activity on cell migration of **RGD-NanoStar/DTX** compared to the free drug in both cell lines at 30 h attested for a good ability of the drug-loaded nanocarrier to reduce tumor propagation and invasiveness, enhancing the typical effect of DTX on metastatization. Overall, **RGD-NanoStar/DTX** specifically inhibited the migratory activity of both tumoral cell lines in a more effective way respect to free DTX at specific drug concentrations, more relevantly on MDA-MB 468 cells, leading to the opportunity to design, in perspective, specific therapeutic strategies.

5. Conclusions

In summary, we designed an efficient multistep route for the synthesis of a novel amphiphilic *star*PLA-PEG copolymer decorated with the tumor-targeting ligand RGD peptide. Specifically, the combination of ROP and *click* chemistry allowed an optimal control over the molecular weight, the hydrophobic:hydrophilic balance, the molecular weight distributions, and the accessibility of chain-end functionalities. The *star*PLA-PEG-RGD bearing a fascinating three-armed *star*-shaped architecture decorated with RGD was conceived as drug delivery system exploiting its capability to encapsulate the antitumoral drug Docetaxel. After the nanoformulation of *star*PLA-PEG-RGD and drug incorporation into the polymeric micelles, we provided a detailed picture of the cell-material interactions. Specifically, the antiproliferative properties of the nanoshuttle, both unloaded and loaded with Docetaxel, were explored focusing on U87 Human Glioblastoma and MDA-MB 468 Human Breast Adenocarcinoma cell lines, as models of two most common primary and metastatic tumors. A special focus was reserved, more specifically, to the inhibition of cell migration that is associated with the process of metastasis. The stronger ability of **RGD-NanoStar/DTX** to reduce tumor propagation and invasiveness compared to the free drug in both cell lines at 30 h attested for an enhanced effect of the drug-loaded nanocarrier on metastatization respect to free DTX. These biological results, together with the absence of toxicity on healthy Ad-MSCs and with the specific interaction and toxicity towards cancer cells, primarily MDA-MB 468 cell line, could be fruitfully exploited for a perspective design of target therapy. Altogether our studies pointed out that *star*-shaped PLA-PEG copolymers offer a great potential in self-assembly of polymeric nanomaterials with tunable chemistry and functionalities. Moreover, the nanoparticle decoration and drug incorporation afforded powerful nanosystems for cutting-edge nanotechnological applications which can be also implemented, in perspective, with the co-entrapment of other bioactive compounds (drugs or genetic materials) to exploit synergistic actions. The use of blended polymer based on *star*PLA-PEG-RGD and *star*PLA-PEG in a 1:9 ratio turned out to be an excellent choice for our nanoformulation considering that even a small amount of grafted RGD peptide proved able to significantly improve the physico-chemical properties, the amphiphilicity and the biological outcomes of our novel *star*-shaped amphiphilic PLA-PEG copolymer. We believe that this is one of the main strengths of our study and one of the main advantages of our nanoformulation that limited the use of expensive RGD peptide.

CRediT authorship contribution statement

Conceptualization: AS; Investigation: SMT, RO, SP, GB, AM, AP; Project administration: AS; Supervision: AS, OC, MM; Writing - original draft: AS, MM; Writing - review & editing: all authors discussed the results and commented on the manuscript.

Data availability

All data required to reproduce these findings are present in the paper and/or in the Supplementary Materials. Additional data related to this paper may be requested from the authors.

Declaration of competing interest

The authors declare that they have no known competing financial interests or personal relationships that could have appeared to influence the work reported in this paper.

Data availability

Data will be made available on request.

Acknowledgments

This study was partially supported by the grant FFABR Unime 2021_Finanziamento Attività di Base della Ricerca di Ateneo_SCALA_ANGELA.

Appendix A. Supplementary data

Supplementary data to this article can be found online at https://doi.org/10.1016/j.bioadv.2022.213043.

References

[1] P. Kubisa, G. Lapienis, T. Biela, Star-shaped copolymers with PLA–PEG arms and their potential applications as biomedical materials, Polym. Adv. Technol. 32 (2021) 3857–3866, https://doi.org/10.1002/pat.5297.

[2] J.M. Ren, T.G. McKenzie, Q. Fu, E.H.H. Wong, J. Xu, Z. An, S. Shanmugam, T. P. Davis, C. Boyer, G.G. Qiao, Star polymers, Chem. Rev. 116 (2016) 6743–6836, https://doi.org/10.1021/acs.chemrev.6b00008.

[3] A. Michalski, M. Brzezinski, G. Lapienis, T. Biela, Star-shaped and branched polylactides: synthesis, characterization, and properties, Prog. Polym. Sci. 89 (2019) 159–212, https://doi.org/10.1016/j.progpolymsci.2018.10.004.

[4] L.-X. Long, J. Zhao, K. Li, L.G. He, X.M. Qian, C.Y. Liu, L.-M. Wang, X.-Q. Yang, J. Sun, Y. Ren, C.-S. Khang, X.-B. Yan, Synthesis of star-branched PLA-b-PMPC copolymer micelles as long blood circulation vectors to enhance tumor-targeted delivery of hydrophobic drugs in vivo, Mater. Chem. Phys. 180 (2016) 184–194, https://doi.org/10.1016/j.matchemphys.2016.05.062.

[5] S.K. Wong, I. Zainol, M.P. Ng, C.H. Ng, I.Hong Ooi, Dendrimer-like AB2-type star polymers as nanocarriers for doxorubicin delivery to breast cancer cells: synthesis, characterization, in-vitro release and cytotoxicity studies, J. Polym. Res. 27 (2020) 190, https://doi.org/10.1007/s10965-020-02089-2.

[6] T. Wu, Y. Cai, X. Zhao, C.X. Ngai, B. Chu, B. Hsiao, M. Hadjiargyrou, R.B. Grubbs, Synthesis and characterization of poly(ethylene oxide)/polylactide/polylysine tri-arm star copolymers for gene delivery, J. Polym. Sci.APolym. Chem. 56 (2018) 635–644, https://doi.org/10.1002/pola.28938.

[7] W. Tao, X. Zeng, T. Liu, Z. Wanga, Q. Xiong, C. Ouyang, L. Huang, L. Mei, Docetaxel-loaded nanoparticles based on star-shaped mannitol-core PLGA-TPGS diblock copolymer for breast cancer therapy, Acta Biomater. 9 (2013) 8910–8920, https://doi.org/10.1016/j.actbio.2013.06.034.

[8] X. Liu, X. Jin, P.X. Ma, Nanofibrous hollow microspheres self-assembled from star-shaped polymers as injectable cell carriers for knee repair, Nat. Mater. 10 (2011) 398–406, https://doi.org/10.1038/nmat2999.

[9] M. Xie, L. Wang, J. Ge, B. Guo, P.X. Ma, Strong electroactive biodegradable shape memory polymer networks based on star-shaped polylactide and aniline trimer for bone tissue engineering, ACS Appl.Mater. Interfaces 7 (2015) 6772–6781, https://doi.org/10.1021/acsami.5b00191.

[10] N. Hadjichristidis, H. Iatrou, M. Pitsikalis, P. Driva, G. Sakellariou, M. Chatzichristidi, Polymers with star-related structures: synthesis, properties, and applications, in: K. Matyjaszewski, M. Möller (Eds.), Polymer Science: A Comprehensive Reference, Volume 6: Macromolecular Architectures And Soft Nano-objects, Elsevier, Amsterdam, 2012, pp. 29–111.

[11] T. Biela, A. Duda, H. Pasch, K. Rode, Star-shaped poly(L-lactide)s with variable numbers of hydroxyl groups at polyester arms chain-ends and directly attached to the star-shaped core – controlled synthesis and characterization, J. Polym. Sci. A Polym. Chem. 43 (2005) 6116–6133, https://doi.org/10.1002/pola.21035.

[12] K. Khanna, S. Varshney, A. Kakkar, Designing miktoarm polymers using a combination of "Click" reactions in sequence with ring-opening polymerization, Macromolecules 43 (2010) 5688–5698, https://doi.org/10.1021/ma100845a.

[13] P.G. Mineo, C. Foti, F. Vento, M. Montesi, S. Panseri, A. Piperno, A. Scala, Salinomycin-loaded PLA nanoparticles: drug quantification by GPC and wave voltammetry and biological studies on osteosarcoma cancer stem cells, Anal. Bioanal. Chem. 412 (2020) 4681–4690, https://doi.org/10.1007/s00216-020-02721-6.

[14] R. Liénard, M. Montesi, S. Panseri, S.M. Dozio, F. Vento, P. Mineo, A. Piperno, J. De Winter, O. Coulembier, A. Scala, Design of naturally inspired jellyfish-shaped cyclo-polylactides to manage osteosarcoma cancer stem cells fate, Mater. Sci. Eng. C 117 (2020), 111291, https://doi.org/10.1016/j.msec.2020.111291.

[15] A. Scala, A. Piperno, S.M. Torcasio, A. Nicosia, P.G. Mineo, G. Grassi, "Clickable" polylactic acids obtained by solvent free intra-chain amidation, Eur. Polym. J. 109 (2018) 341–346, https://doi.org/10.1016/j.eurpolymj.2018.10.004.

[16] A. Scala, A. Piperno, N. Micale, P.G. Mineo, A. Abbadessa, R. Risoluti, G. Castelli, F. Bruno, F. Vitale, A. Cascio, G. Grassi, "Click" on PLGA-PEG and hyaluronic acid: gaining access to anti-leishmanial pentamidine bioconjugates, J. Biomed. Mater. Res. B Appl. Biomater. 106 (8) (2018) 2778–2785, https://doi.org/10.1002/jbm.b.34058.

[17] U.K. Marelli, F. Rechenmacher, T.R.A. Sobahi, C. Mas-Moruno, H. Kessler, Tumor targeting via integrin ligands, Front. Oncol. 3 (2013) 222, https://doi.org/10.3389/fonc.2013.00222.

[18] L. Battistini, K. Bugatti, A. Sartori, C. Curti, F. Zanardi, RGD peptide-drug conjugates as effective dual targeting platforms: recent advances, Eur. J. Org. Chem. 17 (2021) 2506–2528, https://doi.org/10.1002/ejoc.202100240.

[19] D.L. Morse, H. Gray, C.M. Payne, R.J. Gillies, Docetaxel induces cell death through mitotic catastrophe in human breast cancer cells, Mol. Cancer Ther. 4 (2005) 1495–1503, https://doi.org/10.1158/1535-7163.MCT-05-0130.

[20] C. Yewale, D. Baradia, S. Patil, P. Bhatt, J. Amrutiya, R. Gandhi, G. Kore, A. Misra, Docetaxel loaded immunonanoparticles delivery in EGFR overexpressed breast carcinoma cells, J. Drug Deliv. Sci. Technol. 45 (2018) 334–345, https://doi.org/10.1016/j.jddst.2018.03.027.

[21] S.T. Astner, R. Pihusch, C. Nieder, W. Rachinger, H. Lohner, J.C. Tonn, M. Molls, A.-L. Grosu, Extensive local and systemic therapy in extraneural metastasized glioblastoma multiforme, Anticancer Res. 26 (2006) 4917–4920.

[22] L. Gallego-Yerga, I. Posadas, C. de la Torre, J. Ruiz-Almansa, F. Sansone, C. Ortiz Mellet, A. Casnati, J.M. García Fernández, V. Ceña, Docetaxel-loaded nanoparticles assembled from β-cyclodextrin/calixarene giant surfactants: physicochemical properties and cytotoxic effect in prostate cancer and glioblastoma cells, Front. Pharmacol. 8 (2017) 249, https://doi.org/10.3389/fphar.2017.00249.

[23] T. Zwain, J.E. Alder, B. Sabagh, A. Shaw, A.J. Burrow, K.K. Singh, Tailoring functional nanostructured lipid carriers for glioblastoma treatment with enhanced permeability through in-vitro 3D BBB/BBTB models, Mater. Sci. Eng. C 121 (2021), 111774, https://doi.org/10.1016/j.msec.2020.111774.

[24] J.J. Bravo-Cordero, L. Hodgson, J. Condeelis, Directed cell invasion and migration during metastasis, Curr. Opin. Cell Biol. 24 (2) (2012) 277–283, https://doi.org/10.1016/j.ceb.2011.12.004.

[25] L.-Q. Ouyang, L.-J. Li, K.-J. Zhu, X.-C. Qu, Docetaxel inhibits the migration and invasion of breast cancer cells by suppressing filopodia formation, Tumor 33 (9) (2013) 776–780, https://doi.org/10.3781/j.issn.1000-7431.2013.09.005.

[26] X. Feng, X. Xiong, S. Ma, Docetaxel-loaded novel nano-platform for synergistic therapy of non-small cell lung cancer, Front. Pharmacol. 13 (2022), 832725, https://doi.org/10.3389/fphar.2022.832725.

[27] Xiuxiu Wang, Ru Cheng, Zhiyuan Zhong, Facile fabrication of robust, hyaluronic acid-surfaced and disulfide-crosslinked PLGA nanoparticles for tumor-targeted and reduction-triggered release of docetaxel, Acta Biomater. 125 (2021) 280–289, https://doi.org/10.1016/j.actbio.2021.02.044.

[28] E. Ghassami, J. Varshosaz, M. Mirian, A. Jahanian-Najafabadi, HER-2 aptamer-targeted Ecoflex® nanoparticles loaded with docetaxel promote breast cancer cells apoptosis and anti-metastatic effect, IET Nanobiotechnol. 13 (4) (2019) 428–434, https://doi.org/10.1049/iet-nbt.2018.5047.

[29] J. Varshosaz, M.A. Davoudi, S. Rasoul-Amini, Docetaxel loaded nanostructured lipid carriers functionalized with Trastuzumab (Herceptin) for HER2-positive breast cancer cells, J. Liposome Res. 28 (2018) 285–295, https://doi.org/10.1080/08982104.2017.1370471.

[30] P. Rafiei, A. Haddadi, Docetaxel-loaded PLGA and PLGA-PEG nanoparticles for intravenous application: pharmacokinetics and biodistribution profile, Int. J. Nanomedicine 12 (2017) 935–947, https://doi.org/10.2147/IJN.S121881.

[31] Z. Xu, Y. Zhang, Q. Hu, Q. Tang, J. Xu, J. Wu, T.B. Kirk, D. Ma, W. Xue, Biocompatible hyperbranched polyglycerol modified β-cyclodextrin derivatives for docetaxel delivery, Mater. Sci. Eng. C Mater. Biol. Appl. 71 (2017) 965–972, https://doi.org/10.1016/j.msec.2016.11.005.

[32] C. Conte, A. Scala, G. Siracusano, G. Sortino, R. Pennisi, A. Piperno, A. Miro, F. Ungaro, M.T. Sciortino, F. Quaglia, A. Mazzaglia, Nanoassemblies based on non-ionic amphiphilic cyclodextrin hosting Zn(II)-phthalocyanine and docetaxel: design, physicochemical properties and intracellular effects, Colloids Surf. B 146 (2016) 590–597, https://doi.org/10.1016/j.colsurfb.2016.06.047.

[33] D. Zhu, W. Tao, H. Zhang, G. Liu, T. Wang, L. Zhang, X. Zeng, L. Mei, Docetaxel (DTX)-loaded polydopamine-modified TPGS-PLA nanoparticles as a targeted drug delivery system for the treatment of liver cancer, Acta Biomater. 30 (2016) 144–154, https://doi.org/10.1016/j.actbio.2015.11.031.

[34] M. Chang, S. Lu, F. Zhang, T. Zuo, Y. Guan, T. Wei, W. Shao, G. Lin, RGD-modified pH-sensitive liposomes for docetaxel tumor targeting, Colloids Surf. B 129 (2015) 175–182, https://doi.org/10.1016/j.colsurfb.2015.03.046.

[35] A.V. Ponce Bobadilla, J. Arévalo, E. Sarró, H.M. Byrne, P.K. Maini, T. Carraro, S. Balocco, A. Meseguer, T. Alarcón, In vitro cell migration quantification method for scratch assays, J. R. Soc. Interface 16 (2019), 20180709, https://doi.org/10.1098/rsif.2018.0709.

[36] C. Garofalo, G. Capuano, R. Sottile, R. Tallerico, R. Adami, E. Reverchon, E. Carbone, L. Izzo, D. Pappalardo, Different insight into amphiphilic PEG-PLA copolymers: influence of macromolecular architecture on the micelle formation and cellular uptake, Biomacromolecules 15 (2014) 403–415, https://doi.org/10.1021/bm401812r.

[37] O. Coulembier, S. Moins, J.-M. Raquez, F. Meyer, L. Mespouille, E. Duquesne, P. Dubois, Thermal degradation of poly(l-lactide): accelerating effect of residual DBU-based organic catalysts, Polym. Degrad. Stab. 96 (2011) 739–744, https://doi.org/10.1016/j.polymdegradstab. 2011.02.014.

[38] R. Mahou, C. Wandrey, Versatile route to synthesize heterobifunctional poly (ethylene glycol) of variable functionality for subsequent Pegylation, Polymers 4 (2012) 561–589, https://doi.org/10.3390/polym4010561.

[39] S.K. Boopathi, N. Hadjichristidis, Y. Gnanou, X. Feng, Direct access to poly(glycidyl azide) and its copolymers through anionic (co-)polymerization of glycidyl azide, Nat. Commun. 10 (2019) 293, https://doi.org/10.1038/s41467-018-08251-1.

[40] P. Leophairatana, C.C. De Silva, J.T. Koberstein, How good is CuAAC "click" chemistry for polymer coupling reactions? J. Polym. Sci.APolym.Chem. 56 (2018) 75–84, https://doi.org/10.1002/pola.28872.

[41] P. Leophairatana, S. Samanta, C.C. De Silva, J.T. Koberstein, Preventing alkyne-alkyne (i.e., Glaser) coupling associated with the ATRP synthesis of alkyne-functional polymers/macromonomers and for alkynes under click (i.e., CuAAC) reaction conditions, J. Am. Chem. Soc. 139 (2017) 3756–3766, https://doi.org/10.1021/jacs.6b12525.

[42] C. Li, W. Wanga, Y. Xi, J. Wang, J.-F. Chen, J. Yun, Y. Le, Design, preparation and characterization of cyclic RGDfK peptide modified poly(ethylene glycol)-block-poly(lactic acid) micelle for targeted delivery, Mater. Sci. Eng. C 64 (2016) 303–309, https://doi.org/10.1016/j.msec.2016.03.062.

[43] P. Falvey, C.W. Lim, R. Darcy, T. Revermann, U. Karst, M. Giesbers, A.T. Marcelis, A. Lazar, A.W. Coleman, D.N. Reinhoudt, B.J. Ravoo, Bilayer vesicles of amphiphilic cyclodextrins: host membranes that recognize guest molecules, Chem. Eur. J. 11 (2005) 1171–1180, https://doi.org/10.1002/chem.200400905.

[44] H.J. Kreuzer, R.L.C. Wang, M. Grunze, Hydroxide ion adsorption on self-assembled monolayers, J. Am. Chem. Soc. 125 (2003) 8384–8389, https://doi.org/10.1021/ja0350839.

[45] M. Johnsson, A. Wagenaar, J.B.F.N. Engberts, Sugar-based gemini surfactant with a vesicle-to-micelle transition at acidic pH and a reversible vesicle flocculation near neutral pH, J. Am. Chem. Soc. 125 (2003) 757–760, https://doi.org/10.1021/ja028195t.

[46] J.M. Rios De La Rosa, A. Spadea, R. Donno, et al., Microfluidic-assisted preparation of RGD-decorated nanoparticles: exploring integrin-facilitated uptake in cancer cell lines, Sci. Rep. 10 (2020) 14505, https://doi.org/10.1038/s41598-020-71396-x.
[47] W. Tao, X. Zeng, T. Liu, Z. Wang, Q. Xiong, C. Ouyang, L. Huang, L. Mei, Docetaxel-loaded nanoparticles based on star-shaped mannitol-core PLGA-TPGS diblock copolymer for breast cancer therapy, Acta Biomater. 9 (2013) 8910–8920, https://doi.org/10.1016/j.actbio.2013.06.034.
[48] S. Ordanini, F. Cellesi, Complex polymeric architectures self-assembling in unimolecular micelles: preparation,characterization and drug nanoencapsulation, Pharmaceutics 10 (2018) 209, https://doi.org/10.3390/pharmaceutics10040209.
[49] X. Jin, P. Sun, G. Tong, X. Zhu, Star polymer-based unimolecular micelles and their application in bio-imaging and diagnosis, Biomaterials 178 (2018) 738–750, https://doi.org/10.1016/j.biomaterials.2018.01.051.
[50] M. Shibata, M. Matsumoto, Y. Hirai, M. Takenaka, M. Sawamoto, T. Terashima, Intramolecular folding or intermolecular self-assembly of amphiphilic random copolymers: on-demand control by pendant design, Macromolecules 51 (2018) 3738–3745, https://doi.org/10.1021/acs.macromol.8b00570.
[51] B.S. Bolu, B. Golba, N. Boke, A. Sanyal, R. Sanyal, Designing dendron-polymer conjugate based targeted drug delivery platforms with a "Mix-and-Match" modularity, Bioconjug. Chem. 28 (2017) 2962–2975, https://doi.org/10.1021/acs.bioconjchem.7b00595.
[52] I. Martínez-Reyes, N.S. Chandel, Cancer metabolism: looking forward, Nat. Rev. Cancer 21 (2021) 669–680, https://doi.org/10.1038/s41568-021-00378-6.
[53] K.T. Cheng, [18F]FB-NH-mini-PEG-E{E[c(RGDyK)]2}2 [Updated 2008 Mar 12], in: Molecular Imaging And Contrast Agent Database (MICAD), National Center for Biotechnology Information (US), Bethesda (MD), 2008 Feb 20, pp. 2004–2013 [Internet].
[54] T. Sim, J.E. Kim, N.H. Hoang, J.K. Kang, C. Lim, D.S. Kim, E.S. Lee, Y.S. Youn, H.-G. Choi, H.-K. Han, K.-Y. Weon, K.T. Oh, Development of a docetaxel micellar formulation using poly(ethylene glycol)–polylactide–poly(ethylene glycol) (PEG–PLA–PEG) with successful reconstitution for tumor targeted drug delivery, Drug Deliv. 25 (2018) 1362–1371, https://doi.org/10.1080/10717544.2018.1477865.